New Insights into the Inhibition of Human Neutrophil Elastase by Heparin[†]

Jean L. Spencer,[‡] Phillip J. Stone,[‡] and Matthew A. Nugent*[,‡,§,||]

Departments of Biochemistry, Ophthalmology, and Biomedical Engineering, Boston University School of Medicine, Boston, Massachusetts 02118

Received February 17, 2006; Revised Manuscript Received May 25, 2006

ABSTRACT: In the normal feedback mechanism of injury and repair in the lung, fragmented heparan sulfate proteoglycans (HSPGs) from damaged extracellular matrix and cells are believed to interact with elastases to limit their activity. An imbalance in the HSPG−elastase response may play an important role in situations where uncontrolled lung injury leads to diseases such as emphysema. To gain insight into this complex process of heparin and heparan sulfate regulation of elastases, an experimental study was undertaken to resolve the mechanism and structural requirements of heparin inhibition of human neutrophil elastase (HNE). Kinetic analyses were completed using in vitro assays with synthetic and insoluble elastin substrates in the presence of HNE and various heparin preparations (14−15 kDa; 17−19 kDa), heparin-derived oligosaccharides (4−22 saccharides), and chemically modified heparins (2-O-, 6-O-, O-, and N-desulfated). Results showed that heparin inhibits HNE by a tight-binding, hyperbolic, competitive mechanism, contrary to previous reports in the literature. A minimum length of at least 12−14 saccharides is required for inhibition, after which inhibitory activity increases with chain length (or molecular mass). Although all *N*- and *O*-sulfate groups contribute to inhibition, 2-*O*-sulfate groups are less critical than either *N*- or 6-*O*-sulfate groups, indicating that inhibitory activity is dependent upon the heparin fine structure. Molecular-docking simulations support the kinetic results and provide a plausible model for the size requirement, whereby positively charged, clamp-like regions at the ends of the interdomain crevice (elastase fold) are used by heparin to bridge the active site and inhibit activity.

Chronic obstructive pulmonary disease (COPD)[1] is the fourth leading cause of death in the world and is rapidly increasing in many countries (*1*). Despite the prevalence of this disease, COPD is frequently referred to as a "quiet killer" because it progresses very slowly and is often undiagnosed and untreated in early stages (*2*, *3*). Many people with COPD are unaware of its presence until the disease reaches an advanced state. One type of COPD is emphysema, a disease in which the walls of the alveoli are gradually destroyed. As a consequence of this structural damage, the many small air spaces coalesce into larger and fewer air spaces, reducing the overall elasticity of the lungs and decreasing the available surface area for gas exchange between the body and environment. These changes are irreversible, and as they evolve, breathing becomes more and more compromised for the individual.

Elastases released from inflammatory cells such as macrophages and neutrophils play a major role in the tissue damage in emphysematous lungs. Neutrophil elastase, in particular, is a potent enzyme capable of degrading key macromolecular components of connective tissue, including elastin (*4*−*6*). Under conditions of tissue injury, elastase, oxidants, and a defensive array of peptides, proteins, and other enzymes are released into the extracellular matrix by polymorphonuclear neutrophils summoned to the site by inflammatory signals. According to the protease−antiprotease hypothesis, the activity of elastase is balanced by an anti-elastase screen of endogenous inhibitors, with the predominant one being α_1-proteinase inhibitor (*7*−*11*). However, under circumstances of overwhelming stimuli, oxidative inactivation, or genetic deficiency, the natural balance is disrupted and an opportunity develops for elastase to evade local inhibitors, leading to tissue destruction and emphysema.

A proposed option for treating emphysema is to offset the protease−antiprotease imbalance by supplementing the system with artificial elastase inhibitors. Many synthetic and natural inhibitors have been considered for this role, but issues such as toxicity and instability often intrude on continued investigation (*12*, *13*). One inhibitor that circumvents some of these problems is heparin, an anticoagulant drug that has been used in the human body for more than 50 years (*14*). As an inhibitor, heparin is extremely potent against human neutrophil elastases (HNEs), with studies confirming the activity of heparin and heparin derivatives both in vitro (*12*, *13*, *15*−*20*) and in vivo (*13*, *17*, *21*). These studies portray an activity that is highly sensitive to specific properties of the heparin structure (*22*), including molecular

[†] This work was supported by Grant PO1 HL46902 from the National Institutes of Health and by a departmental grant from the Massachusetts Lions Eye Research Fund, Inc.

* To whom correspondence should addressed: Department of Biochemistry, Room K225, Boston University School of Medicine, 715 Albany Street, Boston, MA 02118. Telephone: 617-638-4169. Fax: 617-638-5339. E-mail: mnugent@bu.edu.

[‡] Department of Biochemistry.

[§] Department of Ophthalmology.

[||] Department of Biomedical Engineering.

[1] Abbreviations: CMK, chloromethyl ketone; COPD, chronic obstructive pulmonary disease; HNE, human neutrophil elastase; HSPG, heparan sulfate proteoglycan; PBS, phosphate-buffered saline; PDB, Protein Data Bank.

10.1021/bi060338r CCC: $33.50
Published on Web 07/08/2006

mass and chain length (*18*−*20*), degree of sulfation and charge density (*18*, *19*), specific sulfation (*17*−*19*), and iduronic acid content (*19*, *20*). Research also shows that structural modification of heparin can remove the anticoagulant activity while retaining the inhibitory action, an important factor for potential clinical use (*17*). With increased understanding of these structure−activity relationships, designer molecules based on customized oligosaccharide sequences may become effective therapies for future treatment of emphysema (*14*).

The concept of using heparin to restore the protease−antiprotease balance is of particular interest because the body appears to adopt a similar strategy for local control of elastases within the lung. In this case, however, the supplemental inhibitors are endogenous heparan sulfate proteoglycans (HSPGs), which are present throughout the lungs as components of cell surfaces and the extracellular matrix. These macromolecules consist of a protein core with covalently attached heparan sulfate chains having "heparin-like" regions of high sulfation separated by regions of low sulfation (*23*). As two diverse studies show, one with elastase-treated pulmonary fibroblast cultures (*24*) and another with elastase-induced emphysema in rats (*25*), the exposure of HSPGs to elastase partially cleaves the core protein, releasing free heparan sulfate chains and HSPG fragments. Thus, under mild protease−antiprotease imbalance in the lung, a natural feedback of fragmented HSPGs may contribute to limiting elastase activity. In particular, the high level of HSPGs within basement membranes may help resist elastase-mediated digestion and allow for normal cell and tissue boundaries to be preserved. In conditions of chronic disease, this benefit is likely lost as the pool of HSPGs becomes depleted, tilting the balance in favor of elastase-mediated tissue destruction.

Understanding the role of this in vivo feedback mechanism requires detailed knowledge of the underlying mechanisms of heparin inhibition of elastase. Although there are previous studies on the inhibitory activity of heparin (as described above), there remain considerable gaps in the understanding of the process. For example, heparin is often alluded to as a tight-binding, hyperbolic, noncompetitive inhibitor of elastase, yet there are few studies that actually measure the noncompetitive aspect of this process and the data are somewhat limited (*15*, *18*). In addition, although there is general recognition that *N*- and *O*-sulfate groups of heparin contribute to the inhibition of elastase in a nonequivalent manner, there are confusing claims concerning the relative influence of each of these groups on the overall activity (*17*, *18*). The importance of understanding how elastase activity is controlled, coupled with the limited knowledge of heparin-mediated inhibition, indicates that critical insights will likely be revealed from detailed analyses of heparin inhibition of elastases.

The purpose of this investigation was to undertake a comprehensive in vitro analysis of the inhibition of HNE by heparin to resolve the mechanism and identify the structural requirements. The results from this study support a tight-binding, hyperbolic, competitive mechanism for heparin inhibition of HNE, contrary to previous reports in the literature. Experiments with both synthetic and insoluble elastin substrates show that a chain length of at least 12−14 saccharides is required for inhibition and that all *N*- and *O*-sulfate groups contribute to inhibitory activity, but 2-*O*-sulfate groups are least critical. Molecular-docking simulations support the results of the kinetic analysis and provide a plausible model for the size requirement, whereby positively charged, clamp-like regions at the ends of the interdomain crevice (elastase fold) are used by heparin to bridge the active site and inhibit activity.

EXPERIMENTAL PROCEDURES

Materials

Elastase and Substrates. HNE from purulent sputum (29.5 kDa; EC 3.4.21.37) was purchased from Elastin Products Company, Inc. (Owensville, MO). The elastase protein concentration was determined using a molar absorptivity at 280 nm of 2.91×10^4 M^{-1} cm^{-1} (*26*). The substrate *N*-succinyl-L-alanyl-L-alanyl-L-alanine-*p*-nitroanilide (Suc-Ala_3-*p*NA) was also from Elastin Products. For active-site titration, the substrate *N*-succinyl-L-alanyl-L-alanyl-L-valine-*p*-nitroanilide (Suc-Ala_2-Val-*p*NA) and the active-site-directed irreversible inhibitor *N*-methoxysuccinyl-L-alanyl-L-alanyl-L-prolyl-L-valine chloromethyl ketone (MeO-Suc-Ala_2-Pro-Val-CH_2Cl) were from Sigma−Aldrich Corporation (St. Louis, MO). Elastin was extracted from bovine ligamentum nuchae and was radiolabeled by reduction with NaB^3H_4 (*27*). The resulting ^3H-elastin had a specific activity of 7.0×10^5 dpm/mg (0.32 μCi/mg).

Heparin Inhibitors. Heparin sodium salt derived from porcine intestinal mucosa with an average molecular mass of 17−19 kDa was from Sigma−Aldrich, and heparin with a lower molecular mass of 14−15 kDa was from Neoparin, Inc. (Alameda, CA). Chemically modified heparins consisting of compounds with sulfate groups selectively removed from the 2-O, 6-O, O, and N positions (11−13 kDa), and a series of heparin-derived oligosaccharides consisting of a tetrasaccharide (1.2 kDa), an octasaccharide (2.4 kDa), a decasaccharide (3.0 kDa), and two larger oligosaccharides (oligo I with ∼12 saccharides, 3.5 kDa; and oligo II with ∼14 saccharides, 4.2 kDa) were from Neoparin. The oligosaccharides were produced by controlled deaminative cleavage of heparin and contained a reducing terminal anhydromannitol. Longer oligosaccharides (14 saccharide, 4.7 kDa; 18 saccharide, 6.0 kDa; and 22 saccharide, 7.3 kDa) produced by partial depolymerization of heparin by heparinase I were purchased from V-Labs, Inc. (Covington, LA). The V-Labs compounds were characterized by an unsaturated 2-O-sulfated uronic acid at the nonreducing end.

Other Materials. High-purity salts for buffers were from Sigma−Aldrich and consisted of tris(hydroxymethyl)aminomethane (Tris), Tris hydrochloride (Tris-HCl), sodium chloride (NaCl), potassium phosphate monobasic (KH_2PO_4), and sodium phosphate dibasic (Na_2HPO_4). Dulbecco's phosphate-buffered saline (PBS) without calcium and magnesium salts was from Invitrogen Corporation (Carlsbad, CA). Other buffer components included Brij 35 (American Bioanalytical, Natick, MA), sodium azide (NaN_3; LabChem, Inc., Pittsburgh, PA), dimethyl sulfoxide (DMSO; Sigma−Aldrich), and 1 N hydrochloric acid (HCl; EM Science, Gibbstown, NJ). Milli-Q water was generated in-house with a resistivity greater than 18 MΩ cm.

General Methods

Stock Preparation. All stock solutions of HNE, Suc-Ala_3-*p*NA, and inhibitors were freshly made in buffer. The buffers included Tris-buffered saline (0.10 M Tris/Tris-HCl and 0.093 M NaCl at pH 8.0, ionic strength = 0.15 M at 27 °C), phosphate buffer (0.05 M Na_2HPO_4/KH_2PO_4 at pH 7.4, ionic strength = 0.13 M at 27 °C), and PBS without calcium and magnesium salts (pH 7.1, ionic strength = 0.15 M). An important aspect of stock preparation was the consistent handling of the solutions. The HNE stock solution was gently mixed, placed on ice, and added within 10−12 min to the assay. In contrast, Suc-Ala_3-*p*NA stock solution was vigorously vortexed for 30 s, wrapped with foil, and allowed to stand at room temperature for at least 1 h before use. Substrate solubility was checked by centrifuging at 2000*g* for 15 min at 4 °C, followed by base hydrolysis of the supernatant (*28*) and measurement of the absorbance at 410 nm (4-nitroaniline). Organic solvents were avoided in substrate preparation because HNE activity is sensitive to their presence (*29*). Inhibitor stock solutions were mixed well and kept at room temperature until use. Heparin-derived inhibitors were added to the reaction on a mass basis (instead of a molar basis) to make comparisons based on an equal number of saccharides.

HNE Active-Site Titration. The activity of HNE was determined by titration with the irreversible chloromethyl ketone (CMK) inhibitor MeO-Suc-Ala_2-Pro-Val-CH_2Cl and by measurement of the subsequent activity with the substrate Suc-Ala_2-Val-*p*NA according to a procedure provided by Dr. Antonio Baici (University of Zurich) and adapted for this study. The method was reported to give similar results to those obtained by "burst" active-site titration with azapeptides (*30*). Individual stock solutions of 3.38 μM HNE (on the basis of protein content), 10.0 μM CMK, and 0.70 mM substrate were prepared in phosphate buffer with 2% (w/w) DMSO. A 200 μL volume of HNE stock was mixed with 100 μL of 0.92−5.52 μM CMK solutions to give final solutions having an HNE concentration of 2.25 μM and HNE/CMK molar ratios from 1.2 to 7.3. These solutions, together with an HNE control with no CMK, were preincubated at 27 °C for 35 min. After preincubation, 12 μL of each solution was combined with 238 μL substrate stock in triplicate in a 96-well microplate. The plate was incubated at 27 °C for 1 h in an OPTImax tunable microplate reader (Molecular Devices Corporation, Sunnyvale, CA), and absorbance readings (410 nm) were taken every 30 s after 5 s of shaking. The reaction rates were determined from the linear portion of the absorbance-versus-time plots, and the residual activity of the enzyme was calculated as the average rate of the HNE/CMK sample divided by the average rate of the HNE control.

The data from three active-site titrations were plotted as residual activity versus the CMK concentration (from preincubation). Linear regression of the 16 points ($R^2 = 0.97$) resulted in an *x* intercept of 2.07 μM, the concentration of active sites. From the ratio of this intercept to the HNE concentration (2.25 μM), the activity was determined to be 92 ± 4%. This result was checked against an internal HNE preparation that had a reported activity of 98 ± 4% as determined by titration with *p*-nitrophenyl-3-(*n*-acetyl-L-alanyl-L-alanyl)-2-(1-propyl)-carbazate (*31*). Both samples of HNE were run in the chromogenic substrate assay. The average rate ratio (rate with commercial HNE/rate with internal HNE) for four different substrate concentrations was 0.95, which agreed within experimental error with the value of 0.94 expected from the ratio of active sites. The HNE concentrations reported in this study are based on an activity of 92%.

Heparin/HNE Binding Stoichiometry. The number of HNE molecules that bind to one heparin molecule was determined by titrating the enzyme with heparin. The relative rate of hydrolysis was measured at constant concentrations of HNE and substrate while increasing the amount of heparin. The linear inhibition curve was generated under the constraint $[E]_o/K_i \geq 100$, which guaranteed that almost all of the heparin would be bound to HNE in a pseudo-irreversible manner (*32*). A literature value for K_i of 3.3 nM (*16*) was used to estimate a lower limit for the elastase concentration. Tris-buffered saline and stock solutions of HNE (29 μM), Suc-Ala_3-*p*NA (15 mM), and heparin (2.78 μM; 17−19 kDa) were combined in triplicate in a 96-well microplate to give a set of wells with varying concentrations of heparin and another set without heparin (HNE controls). The final well volume of 250 μL contained 1.16 μM HNE, 1.50 mM substrate, and where appropriate, 0.056−1.67 μM heparin. Absorbance readings (410 nm) were taken every 30 s after 5 s of shaking for 1 h at 27 °C in the microplate reader. Rates were calculated from the linear portion of the curves during the first 15 min of reaction and averaged over triplicate samples. The results were plotted as relative rate (v_i/v_o = rate with heparin/rate without heparin) versus the heparin/HNE molar ratio (0.048−1.44). The *x* coordinate of the intersection of the initial linear portion of the plot and the horizontal line of maximum inhibition was used as the heparin/HNE binding ratio or equivalence point.

Chromogenic Substrate Assays. The HNE activity in the presence of various inhibitors was evaluated from the rate of hydrolysis of the chromogenic substrate Suc-Ala_3-*p*NA. Reactions were set up in a 96-well microplate (250 μL/well) and were typically run at 27 °C for 1 h in the microplate reader. Release of the hydrolytic product 4-nitroaniline was measured optically at 410 nm every 30 s following 5 s of plate shaking. Two types of experiments were carried out with the chromogenic assay, one in which the substrate concentration was varied, while the other components remained constant (substrate−response experiment), and one in which the inhibitor concentration was varied, while the other components remained constant (concentration−response experiment). The general procedure for both experiments was similar. Each microplate was organized to contain a series of samples done in triplicate, a matching set of HNE controls (no inhibitor), and a number of blanks (buffer only). Tris-buffered saline was added to all wells, followed by the row-by-row addition of substrate stock (15 mM), inhibitor stock (25 μg/mL), and HNE stock (390 nM) to the appropriate wells. For the substrate−response experiments, typical well concentrations were 120 nM HNE, 5.0 μg/mL inhibitor, and 0.60−3.6 mM substrate. For the concentration−response experiments, typical concentrations were 120 nM HNE, 1.5 mM substrate, and 0.040−14.5 μg/mL inhibitor. A few runs were also performed at other conditions of temperature (30, 34, and 37 °C), ionic strength (0.075 M), and composition (additives Brij 35 and NaN_3).

Elastin Solubilization Assays. The procedure for the elastin solubilization assay was based on the work of Stone and co-workers (*27*). ^{3}H-Elastin powder was carefully weighed into a glass tube-and-pestle homogenizer. The required volume of PBS (without calcium and magnesium salts) for a final suspension of 1 mg/mL was calculated and added to the homogenizer. After 4 min of agitation, the homogenate was poured into a beaker and stirred vigorously for 5 min. As stirring continued, a pipet with a large-orifice filter tip was used to withdraw 1 mL aliquots into 2 mL microtubes. The tubes were centrifuged at 20000*g* for 10 min at 4 °C, and 950 μL of supernatant was discarded without disturbing the pellet. Replacement volumes of either PBS or PBS plus 10 μL of inhibitor stock solution (500 μg/mL) were added to the insoluble elastin pellets, and the tubes were placed on a rotator (6 rpm) at room temperature for 30 min. At the end of the equilibration period, 10 μL of HNE stock solution (12 μM) was added to all tubes except the elastin controls. After this final step, each tube contained 1 mL of buffer with 1.0 mg/mL ^{3}H-elastin, and where appropriate, 120 nM HNE and 5.0 μg/mL inhibitor. The tubes were incubated on a rotator (6 rpm) at 37 °C for 2 h. After incubation, the tubes were placed on ice until the contents were transferred to centrifugal filter units (Millipore Ultrafree-CL, 5.0 μm). The filters were centrifuged at 4000*g* for 4 min at 4 °C. A 100 μL sample was taken from each filtrate collection tube and thoroughly mixed with a 5 mL scintillation cocktail. Radioactivity was measured with a Packard 1900 TR liquid scintillation spectrometer (Packard Instrument Company, Meriden, CT). Measurements of triplicate samples were averaged and corrected for the background (nonspecific release of tritium) by subtracting the average of the elastin controls. The corrected results were used to calculate the relative rate (v_i/v_o = ^{3}H-elastin digestion with the inhibitor/^{3}H-elastin digestion without the inhibitor) of released tritium at each condition.

Molecular Docking. All molecular structure files were obtained from the Protein Data Bank (PDB) (*33*). The structure for HNE was taken from PDB file 1HNE (*34*). The crystal in this file is a complex between HNE and the CMK inhibitor MeO-Suc-Ala$_2$-Pro-Ala-CH$_2$Cl with coordinates determined by X-ray diffraction at 1.84 Å resolution. Although two other PDB files were considered for HNE (*35*, *36*), this file was chosen because of the good resolution and the similarity of the small peptide inhibitor with the synthetic substrate of this study. All data records for the inhibitor and for water molecules were manually removed from the file, and the edited version was used as the receptor input to the molecular-docking program. The numbering of the amino acid residues was retained from the original PDB file and corresponded by convention with the sequence of bovine chymotrypsinogen A (*37*).

The structure for heparin was represented by a dodecasaccharide, the largest heparin-derived oligosaccharide in the PDB database. The file 1HPN contains two solution conformers of the dodecasaccharide obtained by nuclear magnetic resonance (NMR) spectroscopy (*38*). The records for the two structures ($^1C_4$ chair and $^2S_0$ skew-boat conformers) were split into separate files, and all hydrogen atoms were manually deleted from each file. The resulting heparin dodecasaccharide structures were used to generate a pair of hexasaccharides by removing six sugar residues from each conformer. The $^1C_4$ conformers of the dodecasaccharide and hexasaccharide were the main ligands evaluated in the docking program.

To gain some insight into the binding patterns of heparin on the elastase surface, an initial-stage molecular-docking program was implemented for this study. ZDOCK 2.3 is an automated algorithm for rigid-body docking that fully explores three rotational and three translational degrees of freedom (*39*−*41*). The grid-based program explicitly searches the entire rotational space and uses a fast Fourier transform to search the translational space. A small amount of conformational flexibility is allowed by tolerating some overlap of the receptor and the ligand structures (soft docking). The scoring function is a linear combination of pairwise shape complementarity, desolvation, and electrostatics. The atomic parameters required for the scoring function (radius, partial charge, and type based on atomic contact energies) are automatically assigned for proteins and manually specified in the case of oligosaccharides. The ZDOCK output contains 2000 predicted complexes ranked in order from best to worst.

The executable code for ZDOCK was downloaded from the Web (http://zlab.bu.edu) onto an Intel Pentium 3 computer running Linux, and molecular structures were visualized with Protein Explorer 2.45 (*42*), a Web-interactive viewer (http://proteinexplorer.org). The top 10 predictions from each docking run were displayed as space-filling models with van der Waals surfaces. Because electrostatic interactions between arginine residues on HNE and sulfate groups on the oligosaccharide are important for binding (*22*), the ionic contacts for each complex were determined by manually counting appropriate atoms within about 0.4 nm (4 Å) of each other. Predictions were evaluated on the basis of the number of ionic contacts and the general location of the docked oligosaccharide. Although a more detailed analysis was considered, this simpler evaluation seemed appropriate for complexes generated by an initial-stage docking program.

Theory−*Enzyme Kinetics*. Evidence in the literature (*15*, *18*, *19*) indicates that inhibition of HNE hydrolysis of Suc-Ala$_3$-*p*NA by various heparin compounds follows a tight-binding, hyperbolic mechanism. The general scheme for hyperbolic inhibition is

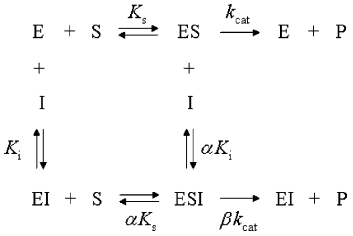

where E is the enzyme, S is the substrate, P is the product, and I is the inhibitor (*43*, *44*). The important point about hyperbolic inhibition is that the product forms not only from the ES complex but also from the ESI complex. Because of this fact, increasing the concentration of I will never completely inhibit the formation of the product. The other parameters in the inhibition scheme include K_s, the dissociation constant of the ES complex; K_i, the dissociation constant of the EI complex; k_{cat}, the rate constant for breakdown of the ES complex; and α and β, two dimensionless factors representing changes in binding affinity and catalytic activity, respectively, in the presence of the inhibitor. Under the condition of hyperbolic inhibition, α and β have values of 0

$< \alpha < \infty$ and $0 < \beta \leq 1$. Dependent upon the particular values of these factors, the inhibitory mechanism can be further classified as competitive ($\beta = 1$, $1 < \alpha < \infty$), noncompetitive ($\alpha = 1$, $0 < \beta < 1$), or mixed (*44*).

In the development of the rate equation for hyperbolic inhibition, the additional aspect of tight binding plays a significant role in making the derivation more complex. Because the enzyme has high affinity for the inhibitor, the depletion of the inhibitor concentration must be taken into account. This consideration is included in the steady-state rate equation for tight-binding, hyperbolic inhibition as derived by Szedlacsek and colleagues (*45*)

$$\frac{v_i}{v_o} = \left(\frac{v_o - v_\infty}{2v_o}\right)\left\{\left[\left(\frac{1+\sigma}{\alpha+\sigma}\frac{\alpha K_i}{[E^*]_o} + \frac{[I^*]_o}{[E^*]_o} - 1\right)^2 + 4\frac{1+\sigma}{\alpha+\sigma}\frac{\alpha K_i}{[E^*]_o}\right]^{1/2} + \frac{v_o + v_\infty}{v_o - v_\infty} - \frac{1+\sigma}{\alpha+\sigma}\frac{\alpha K_i}{[E^*]_o} - \frac{[I^*]_o}{[E^*]_o}\right\} \quad (1)$$

with

$$\frac{v_\infty}{v_o} = \beta\frac{1+\sigma}{\alpha+\sigma} \quad (2)$$

and

$$\sigma = \frac{[S]_o}{K_m} \quad (3)$$

where v_i is the rate in the presence of the inhibitor, v_o is the rate in the absence of the inhibitor, v_∞ is the limit of v_i for a saturating concentration of the inhibitor, $[E^*]_o$ is the initial concentration of binding sites on the enzyme, $[I^*]_o$ is the initial concentration of binding sites on the inhibitor, and σ is the ratio of the initial substrate concentration, $[S]_o$, to the Michaelis constant, K_m, for the system without the inhibitor. For an inhibitor/enzyme system that has a binding stoichiometry of *n*, where *n* is the number of enzyme molecules that bind to one inhibitor molecule, $[E^*]_o$ is equal to the initial enzyme concentration, $[E]_o$, and $[I^*]_o$ is equal to the initial inhibitor concentration, $[I]_o$, multiplied by *n*.

As the concentration of the inhibitor increases, the fraction of bound inhibitor becomes small compared with the total amount of inhibitor. Eventually, even though the inhibitor is tight-binding, the assumption of the constant inhibitor concentration becomes valid and the standard hyperbolic rate equation is applicable (*44*)

$$v_i = \frac{V_{max}\left(\frac{1 + \frac{\beta[I]_o}{\alpha K_i}}{1 + \frac{[I]_o}{\alpha K_i}}\right)[S]_o}{K_m\left(\frac{1 + \frac{[I]_o}{K_i}}{1 + \frac{[I]_o}{\alpha K_i}}\right) + [S]_o} \quad (4)$$

where K_m and V_{max} are the Michaelis−Menten parameters for the system without the inhibitor.

When $[I]_o \gg K_i$, eq 4 reduces to

$$v_i = \frac{\beta V_{max}[S]_o}{\alpha K_m + [S]_o} \quad (5)$$

or

$$v_i = \frac{V_{max}^{app}[S]_o}{K_m^{app} + [S]_o} \quad (6)$$

where K_m^{app} and V_{max}^{app} are the apparent Michaelis constant and the apparent maximal velocity, respectively, in the system with a saturating concentration of inhibitor. Thus, the values of α and β can be determined from the ratios

$$\alpha = \frac{K_m^{app}}{K_m} \quad (7)$$

$$\beta = \frac{V_{max}^{app}}{V_{max}} \quad (8)$$

Calculation of Kinetic Parameters. The data from the chromogenic substrate assay consisted of absorbance readings in triplicate as a function of time. At each time point, the readings were averaged and a blank (buffer only) was subtracted to give a corrected average absorbance. Substrate and substrate/inhibitor controls (no enzyme) were not used because they had a negligible effect on rate calculations (substrate autohydrolysis was less than 0.1% of the slowest rate in the presence of enzyme). The corrected average absorbance was plotted as a function of time to check for linearity. The steady-state reaction rate, v, was determined from the slope of the plot over a 20 min period at least 20 min after the start of the reaction to allow for temperature equilibration. Product formation during the reaction was usually less than 5% of the initial substrate concentration. Calibration of the microplate reader with 4-nitroaniline solutions gave an absorbance conversion factor of 1.83×10^{-4} M.

Two programs to implement nonlinear regression of the experimental data were written with Absoft Pro Fortran 7.5 for Windows (Absoft Corporation, Rochester Hills, MI) and run on an Intel Pentium 4 computer. The least-squares fit of the data was performed with the double-precision, IMSL routine DRNLIN using a modified Levenberg−Marquardt algorithm (*46*). The output from each program gave the best-fit values and standard errors of the unknown parameters. The first program handled the substrate−response experiments and fit the data ($[S]_o$, v) to the Michaelis−Menten equation with two adjustable parameters, K_m and V_{max} (or K_m^{app} and V_{max}^{app}). The values of K_m, V_{max}, K_m^{app}, and V_{max}^{app} were used to calculate α and β for each run. The second program was designed for the concentration−response experiments and included an option for selecting up to three adjustable parameters. The experimental data ($[I]_o$, v_i/v_o) were fit to eq 1 by adjusting the parameter K_i alone or in combination with one other parameter ($[E]_o$, *n*, or α).

RESULTS

Mechanism of Heparin Inhibition of HNE Hydrolysis. Figure 1 shows the results of substrate−response experiments for HNE hydrolysis of Suc-Ala_3-*p*NA in the absence and

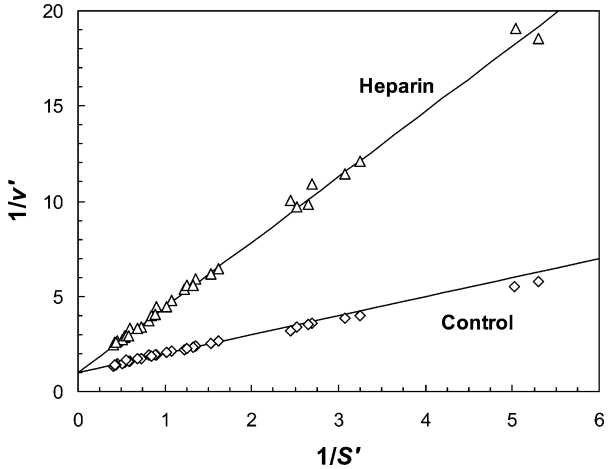

FIGURE 1: Double-reciprocal plot for heparin inhibition of HNE hydrolysis of Suc-Ala$_3$-*p*NA at 27 °C. Reaction conditions: $[E]_o$ = 120 nM; $[I]_o$ = 280 nM (5.0 μg/mL; 17−19 kDa); $[S]_o$ = 0.30−3.6 mM; buffer = 0.10 M Tris/Tris-HCl and 0.093 M NaCl (pH 8.0, ionic strength = 0.15 M at 27 °C); T = 27 °C; t = 1 h; V = 250 μL. Selected data points (average of triplicate readings) are shown for 6 runs: heparin (△); control (◇). Lines were generated for heparin from $1/v' = [(K_m^{app}/K_m)/(V_{max}^{app}/V_{max})]\ 1/S' + [1/(V_{max}^{app}/V_{max})]$ and for the control from $1/v' = 1/S' + 1$. Average kinetic parameters were determined from 19 heparin runs and 59 control runs (Table 1). Normalized plot variables: $v' = v/V_{max}$; $S' = [S]_o/K_m$.

presence of 280 nM (5.0 μg/mL; 17−19 kDa) of heparin. The data are displayed in the form of a double-reciprocal plot of $1/v'$ versus $1/S'$, where v' is the normalized rate, v/V_{max}, and S' is the normalized substrate concentration, $[S]_o/K_m$. A total of 19 independent runs were completed, and a representative sample of data from 6 runs is plotted in the graph. For each run, the best-fit values of K_m, K_m^{app}, V_{max}, and V_{max}^{app} were determined by nonlinear regression of the data to the Michaelis−Menten equation, and the results were used to normalize the data and calculate the ratios K_m^{app}/K_m and V_{max}^{app}/V_{max}. The average values of the ratios from all of the runs were used to generate the displayed line for heparin: $1/v' = [(K_m^{app}/K_m)/(V_{max}^{app}/V_{max})]\ 1/S' + [1/(V_{max}^{app}/V_{max})]$. The line for the control (without heparin) was generated from the relation: $1/v' = 1/S' + 1$. A summary of all parameters for both conditions is given in Table 1. The interesting feature of Figure 1 is the intersection of both lines at a common *y* intercept, a clear indication that heparin inhibits HNE by a competitive mechanism.

In Figure 2A, the influence of increasing amounts of heparin on HNE hydrolysis of Suc-Ala$_3$-*p*NA is depicted in a concentration−response plot of the relative rate, v_i/v_o, versus the concentration. The data represent three independent experiments in which the concentration of heparin was varied from 2.2 to 810 nM (0.040−14.5 μg/mL). The concentrations of HNE and substrate were constant at 120 nM and 1.5 mM, respectively. As the figure shows, the activity of HNE dramatically decreased with an increasing concentration of heparin up to about 100 nM. After this point, increasing amounts of heparin had a diminishing effect on the activity and the relative rate eventually leveled off at about 0.44 or 56% inhibition. The characteristics of this plot denote heparin as a tight-binding, hyperbolic inhibitor of HNE under the conditions of the experiment. The tight-binding aspect of the interaction is supported by the significant inhibition at heparin concentrations much less than the HNE concentration of 120 nM (*32*, *47*). The hyperbolic (or partial) nature of the inhibition is expressed in the failure of increasing amounts of heparin to drive the reaction to zero velocity (*44*).

Because heparin operates as a tight-binding, hyperbolic inhibitor of HNE, the data in Figure 2A were fit to eq 1 to determine K_i. The concentrations of $[E]_o$ and $[S]_o$ were system constants. The value of K_m was taken from Table 1. The values of α and β were set equal to the ratios K_m^{app}/K_m and V_{max}^{app}/V_{max}, respectively, in Table 1. This was justified by the results of Figure 2A showing maximal inhibition at a heparin concentration of 280 nM, the same concentration used to generate the data of Table 1. The value of β was subsequently rounded to 1 to indicate the competitive nature of the inhibition mechanism.

A value for n was estimated by titrating HNE with heparin as illustrated in Figure 2B, where the relative rate, v_i/v_o, is plotted against the molar ratio of heparin/HNE. The higher enzyme concentration (1.16 μM) used in this experiment resulted in less inhibition when compared with the activity in Figure 2A, and a higher quantity of heparin was needed to achieve a similar level of inhibition. This trend is often used as a diagnostic for tight-binding inhibition because neither classical nor hyperbolic inhibition is dependent upon the initial enzyme concentration (*43*, *48*). With a heparin concentration ranging from 0.056 to 1.67 μM, the results in Figure 2B showed a relative rate that is linear up to about 80% of maximum inhibition. The linear part of the curve intersects the horizontal line of maximal inhibition at the x coordinate of 0.311. The reciprocal of this equivalence point suggests that 3.2 molecules of HNE bind to 1 molecule of heparin (17−19 kDa). The value of n was set equal to 3.2. These binding sites were assumed equivalent and independent based on the linearity of the titration curve. For eq 1, $[I^*]_o$ was replaced with $n[I]_o$ or 3.2 $[I]_o$ and $[E^*]_o$ was replaced with $[E]_o$.

With all of the parameters fixed except K_i, the 14 experimental ($[I]_o$, v_i/v_o) pairs were fit to eq 1 by nonlinear regression. The resulting best-fit value (±standard error) for K_i was 6.8 ± 1.8 nM. The curve in Figure 2A was generated using this best-fit value, and a summary of all of the parameters used in fitting the data is given in Table 2. The $[E]_o/K_i$ ratio of 18 falls within the desirable range of $0.01 < [E]_o/K_i < 100$ for determining the K_i of tight binders (*32*). Although a somewhat better fit of the data might be desirable (the residuals are not randomly distributed about the curve), the value for K_i is not unreasonable, especially for a tight-binding inhibitor (*49*). In fact, Frommherz and colleagues (*16*) reported a very similar value of K_i (3.3 ± 1.0 nM) with n equal to 3 for heparin (13.5−15 kDa) and HNE.

As an example of what a better fit might entail, the nonlinear regression routine was repeated on the data set, freeing the constraints on $[E]_o$, n, and α and allowing each one to vary with K_i. Because of the linkage between the terms in eq 1, the variation of either pair (K_i, $[E]_o$) or (K_i, n) resulted in the same regression curve. This curve (- - -) is plotted with the previous regression curve (—) in Figure 2C, which shows the tight-binding region of Figure 2A. The regression curve for the adjustable pair (K_i, α) is not shown because it approximated the fit obtained by varying K_i alone (—). In

Table 1: Kinetic Parameters for Heparin Inhibition of HNE Hydrolysis of Suc-Ala$_3$-*p*NA at 27 °C[a]

	runs[b]	K_m (mM)	V_{max} (10^{-8} M s^{-1})	k_{cat}[c] (s^{-1})	k_{cat}/K_m (M^{-1} s^{-1})	α K_m^{app}/K_m	β V_{max}^{app}/V_{max}
control[d]	59	1.61 ± 0.03[e]	4.36 ± 0.03	0.363 ± 0.003	228 ± 3		
heparin[f]	19	5.94 ± 0.12	4.37 ± 0.08	0.364 ± 0.006	61.4 ± 0.8	3.50 ± 0.07	1.02 ± 0.02

[a] Reaction conditions: $[E]_o$ = 120 nM; $[I]_o$ = 280 nM (5.0 μg/mL; 17−19 kDa); $[S]_o$ = 0.30−3.6 mM; buffer = 0.10 M Tris/Tris-HCl and 0.093 M NaCl (pH 8.0, ionic strength = 0.15 M at 27 °C); T = 27 °C; t = 1 h; V = 250 μL. [b] Number of runs; each run done in triplicate. Total for the control consists of all runs paired with runs for heparin and heparin derivatives in this study. [c] $k_{cat} = V_{max}/[E]_o$. [d] The control has no heparin. [e] Estimated mean ± standard error of the mean. [f] Values for heparin system are apparent kinetic parameters: K_m^{app}, V_{max}^{app}, and k_{cat}^{app}.

this case, the best-fit value for α was the same as the experimentally determined number. The values for all parameters involved in these regressions are listed in Table 2. The best-fit results suggest that a larger experimental value for n, a smaller value for $[E]_o$, or some in-between combination of both would improve the original fit. It is possible that n might be larger, considering the wide distribution of molecular sizes in the heparin preparation. It is also possible that $[E]_o$ might be lower, considering the tendency of HNE to lose activity with time. However, because there is no physical evidence to support either of these suggestions, the most reasonable choice is to accept the K_i based on experimentally determined parameters.

The characteristic response curve in Figure 2A, which shows heparin to be a tight-binding, hyperbolic inhibitor of HNE, has been documented by others (*15*, *18*−*20*, *22*). On the basis of findings reported in two of these studies (*15*, *18*), there is general acceptance that the mode of inhibition is noncompetitive. The only published data appear to be in the study by Redini and associates (*18*), who showed noncompetitive behavior for the inhibition of rat leukocyte elastase by oversulfated heparin hexadecasaccharide and referred to similar results (unpublished) with heparin. In a later study by Baici and co-workers (*15*), this mechanism was extended to the inhibition of human leukocyte elastase by heparin (12 kDa) but the diagnostic plot was not published with the study.

The results in Figure 1 are contrary to this accepted mechanism and clearly identify heparin inhibition of HNE as a competitive mechanism. The reason for this disparity is not obvious. In the process of comparing the present work with the previous two studies (*15*, *18*), some differences in experimental conditions were noted, including (1) a higher reaction temperature (37 °C), (2) a Tris buffer with a lower ionic strength (0.05−0.08 M), (3) the presence of additives (Brij 35, NaN_3), (4) a preincubation period for HNE and heparin before substrate addition, and (5) no agitation during the reaction. These factors were subsequently screened by running substrate−response experiments at each condition. Two additional temperatures (30 and 34 °C) were also included in the screening. The kinetic parameters produced by these analyses are summarized in Table 3. At all conditions, the characteristics of competitive inhibition were obvious in the apparent increase in K_m ($\alpha > 1$) and the lack of change in V_{max} ($\beta = 1$). These results did not provide any evidence for a switch in the mechanism as a consequence of different conditions, and the reason for the discrepancy with the past studies remains unresolved.

Thermodynamics of HNE Hydrolysis. The measurement of kinetic parameters at four different temperatures (Tables 1 and 3) provided the means for estimating thermodynamic properties for two steps in the hydrolysis reaction. The first step was the binding of the enzyme and the substrate: E + S ⇆ ES. Because HNE hydrolysis of Suc-Ala$_3$-*p*NA is controlled by acylation (*29*), the value of K_m is equal to the dissociation constant, K_s, of the ES complex and the reciprocal of K_m is the equilibrium constant for enzyme−substrate binding. In Figure 3A, the logarithm of $1/K_m$ is plotted as a function of the reciprocal of the absolute temperature, $1/T$, according to the van't Hoff equation. The data were fit by straight lines in the presence ($R^2 = 0.96$) and absence ($R^2 = 0.97$) of heparin over a temperature range of 27−37 °C. From the slope of the control (no heparin), the standard enthalpy change, $\Delta H°$, was determined to be −56 kJ mol^{-1}. Additional calculations gave a standard free-energy change, $\Delta G°$, of −16 kJ mol^{-1} (from K_m in Table 1) and a standard entropy change, $\Delta S°$, of −0.13 kJ mol^{-1} K^{-1} (from $\Delta G°$ and $\Delta H°$) at 27 °C. Although $\Delta S°$ is negative and unfavorable ($-T\Delta S° = 40$ kJ mol^{-1}), the enzyme−substrate binding is driven by the large, exothermic $\Delta H°$. The value of $\Delta G°$ is in the range for rapid equilibrium systems (−11 to −34 kJ mol^{-1}) (*44*), and the negative value favors complex formation. For a comparison, this $\Delta G°$ is almost 3-fold smaller than the $\Delta G°$ of −47 kJ mol^{-1} (from $K_i = 6.8$ nM) for the tight-binding interaction between HNE and heparin. The values of $\Delta H°$, $\Delta G°$, and $\Delta S°$ are tabulated in Table 4. The values for the system with heparin are also included, but because K_m^{app} is not equal to K_s, the values represent apparent thermodynamic properties.

The acylation of the ES complex was the second step of the hydrolysis reaction for which a thermodynamic property was determined. Because this step is rate-controlling, V_{max} is proportional to the rate constant for acylation. Figure 3B shows a plot of the logarithm of V_{max} versus $1/T$ according to the Arrhenius relation. The results are linear in the presence and absence of heparin ($R^2 = 0.999$) and have approximately the same slopes as expected from competitive inhibition. On the basis of the best-fit line for the combined data, an activation energy, E_a, of 74 kJ mol^{-1} was calculated for the acylation step. The linearity of the data implies that the rate-controlling step for HNE hydrolysis does not change within this temperature range (*50*).

Effect of Heparin Oligosaccharides on HNE Hydrolysis. Figure 4 illustrates the effect of the chain length on the ability of heparin to inhibit HNE hydrolysis of Suc-Ala$_3$-*p*NA. Heparin-derived oligosaccharides consisting of 4, 8, 10, ∼12, 14, ∼14, 18, and 22 saccharides were added to the reaction system at a concentration of 5.0 μg/mL. Measurements from 2 to 5 runs were collected on each oligosaccharide, and the data were treated in the same manner as described for heparin (Figure 1). Results for the average best-fit values of the kinetic parameters (K_m^{app} and V_{max}^{app}) and the ratios (K_m^{app}/K_m

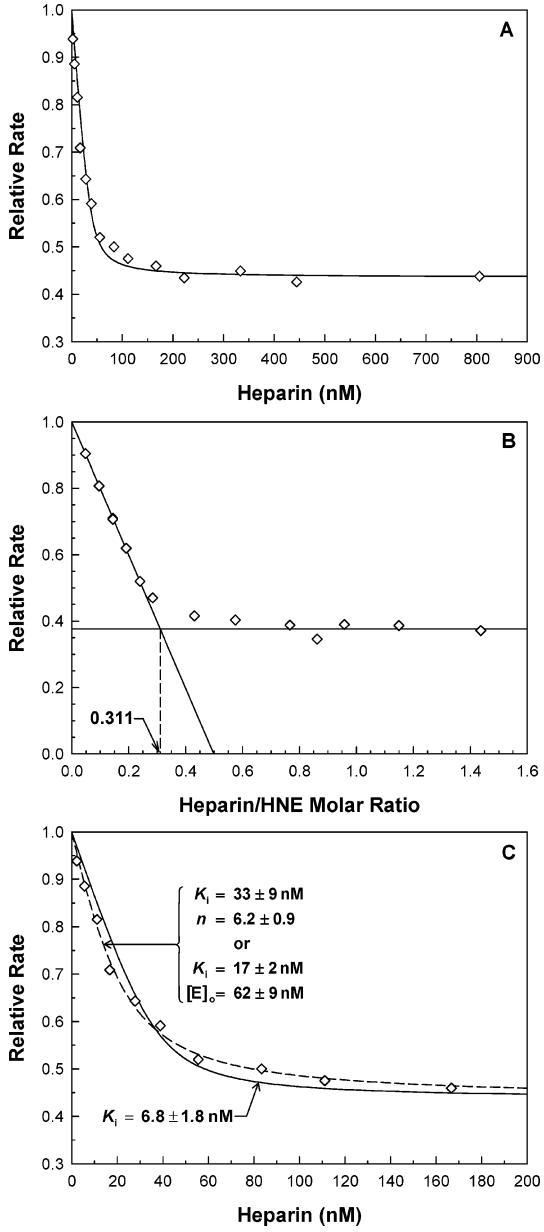

FIGURE 2: (A) Concentration−response plot for heparin inhibition of HNE hydrolysis of Suc-Ala$_3$-*p*NA at 27 °C. Reaction conditions: $[E]_o = 120$ nM; $[I]_o = 2.2-810$ nM (0.040−14.5 μg/mL; 17−19 kDa); $[S]_o = 1.5$ mM; buffer = 0.10 M Tris/Tris-HCl and 0.093 M NaCl (pH 8.0, ionic strength = 0.15 M at 27 °C); $T = 27$ °C; $t = 1$ h; $V = 250$ μL. Data points (average of triplicate readings) are shown for 3 runs. The line was generated by fitting data to eq 1 by nonlinear regression with one adjustable parameter (K_i) and fixed parameters listed in Table 2. Best-fit value of $K_i = 6.8 \pm 1.8$ nM ($n = 3.2$). Relative rate (v_i/v_o) = (rate with heparin)/(rate without heparin); percent inhibition = $(1 - v_i/v_o) \times 100$. (B) Titration curve for determination of heparin/HNE binding stoichiometry at 27 °C. Reaction conditions: $[E]_o = 1.16$ μM; $[I]_o = 0.056-1.67$ μM (1.0−30 μg/mL; 17−19 kDa); $[S]_o = 1.5$ mM; buffer = 0.10 M Tris/Tris-HCl and 0.093 M NaCl (pH 8.0, ionic strength = 0.15 M at 27 °C); $T = 27$ °C; $t = 1$ h; $V = 250$ μL. Data points (average of triplicate readings) are shown for 2 runs. Reciprocal of equivalence point (0.311) = 3.2 molecules of HNE/1 molecule of heparin (17−19 kDa). (C) Nonlinear regression results for heparin inhibition of HNE hydrolysis of Suc-Ala$_3$-*p*NA at 27 °C showing the tight-binding region of Figure 2A. The solid line was generated by fitting data to eq 1 by nonlinear regression with one adjustable parameter: $K_i = 6.8 \pm 1.8$ nM. The dashed line was generated by fitting data with two adjustable parameters: $K_i = 33 \pm 9$ nM, $n = 6.2 \pm 0.9$ or $K_i = 17 \pm 2$ nM, $[E]_o = 62 \pm 9$ nM. Fixed parameters are listed in Table 2.

Table 2: Nonlinear Regression Results for Heparin Inhibition of HNE Hydrolysis of Suc-Ala$_3$-*p*NA at 27 °C[a]

	fixed parameters[b]			best-fit values			
adjustable parameters	α	$[E]_o$ (nM)	n	α	$[E]_o$ (nM)	n	K_i (nM)
K_i	3.50	120	3.2				6.8 ± 1.8[c]
K_i, $[E]_o$	3.50		3.2		62 ± 9		17 ± 2
K_i, n	3.50	120				6.2 ± 0.9	33 ± 9
K_i, α		120	3.2	3.47 ± 0.15			6 ± 3

[a] Experimental conditions: $[E]_o = 120$ nM; $[I]_o = 2.2-810$ nM (0.040−14.5 μg/mL; 17−19 kDa); $[S]_o = 1.5$ mM; buffer = 0.10 M Tris/Tris-HCl and 0.093 M NaCl (pH 8.0, ionic strength = 0.15 M at 27 °C); $T = 27$ °C; $t = 1$ h; $V = 250$ μL. [b] Additional fixed parameters: $K_m = 1.61$ mM; $\beta = 1$; $[S]_o = 1.5$ mM; $M_r = 18\,000$. [c] Best-fit value ± standard error.

Table 3: Screening Results for Heparin Inhibition of HNE Hydrolysis of Suc-Ala$_3$-*p*NA[a]

	control[b]		heparin			
condition	K_m (mM)	V_{max} (10^{-8} M s^{-1})	K_m^{app} (mM)	V_{max}^{app} (10^{-8} M s^{-1})	α K_m^{app}/K_m	β V_{max}^{app}/V_{max}
$T = 30$ °C[c]	1.93	5.67	6.47	5.71	3.43	1.01
$T = 34$ °C	2.44	8.14	7.81	8.66	3.17	1.05
$T = 37$ °C	3.38	10.9	9.79	11.7	2.90	1.08
$I = 0.075$ M[d]	6.43	5.29	13.0	5.40	2.02	1.02
Brij 35/NaN_3[e]	2.03	8.35	7.52	7.99	3.70	0.96
preincubation[f]	1.42	3.90	5.06	3.92	3.58	1.00
no agitation	1.70	5.25	6.23	5.31	3.66	1.01

[a] Standard reaction conditions: $[E]_o = 120$ nM; $[I]_o = 280$ nM (5.0 μg/mL; 17−19 kDa); $[S]_o = 0.60-7.2$ mM; buffer = 0.10 M Tris/Tris-HCl and 0.093 M NaCl (pH 8.0, ionic strength = 0.15 M at 27 °C); $T = 27$ °C; $t = 1$ h; $V = 250$ μL. [b] The control has no heparin. [c] Buffers were adjusted to give pH 8.0 and ionic strength of 0.15 M at reaction temperature: 0.10 M Tris/Tris-HCl and 0.097 M NaCl (30 °C); 0.10 M Tris/Tris-HCl and 0.10 M NaCl (34 °C); 0.10 M Tris/Tris-HCl and 0.11 M NaCl (37 °C). [d] Low ionic strength buffer: 0.10 M Tris/Tris-HCl and 0.019 M NaCl (pH 8.0, ionic strength = 0.075 M at 27 °C). [e] Additives in buffer: 0.01% (w/w) Brij 35; 0.02% (w/w) NaN_3. [f] Preincubation: HNE and heparin for 20 min at 27 °C before the addition of the substrate.

and V_{max}^{app}/V_{max}) are given in Table 5. The data and the associated regression lines are displayed in the double-reciprocal plot of Figure 4A for the oligosaccharides and for a second heparin sample (14−15 kDa; ~48 saccharides). Dashed lines are included as references for the original heparin (17−19 kDa; ~60 saccharides) and the control from Figure 1. As Figure 4A shows, all of the lines intersect at a common *y* intercept, the characteristic indicator of competitive inhibition.

In accordance with a competitive mechanism, the values of V_{max}^{app}/V_{max} (or β) were approximately equal to 1 for all of the compounds. However, the values of K_m^{app}/K_m (or α), which varied from 1 to 3.4, are plotted in Figure 4B as a function of the chain length (number of saccharides). With an α value of about 1, the 4, 8, and 10 saccharides exhibited no inhibition. The ~12-saccharide preparation, which most likely contains chains both larger and smaller than 12 sugars, appeared to span the critical chain length required for activity. Above 12 saccharides, the value of α increased in a linear manner with increasing chain length from 14 to 22 saccharides. The similar α values for 18- and ~14-saccharide chains suggested that the latter preparation contains some 18-sugar

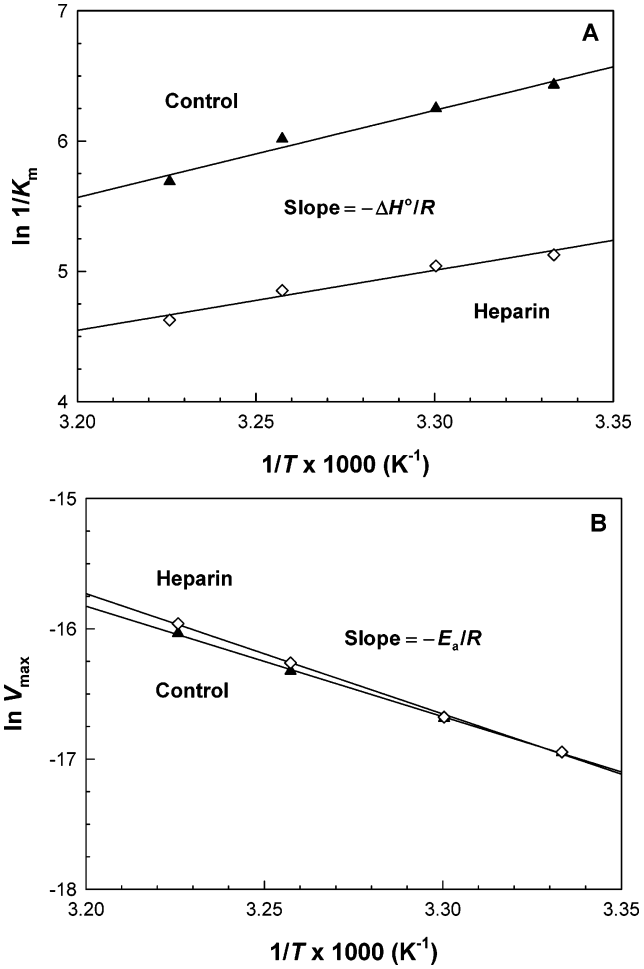

FIGURE 3: Reciprocal temperature plots for estimating $\Delta H°$ and E_a for specific steps in HNE hydrolysis of Suc-Ala$_3$-*p*NA at 27−37 °C. Reaction conditions: $[E]_o = 120$ nM; $[I]_o = 280$ nM heparin (5.0 μg/mL; 17−19 kDa); $[S]_o = 0.30-7.2$ mM; buffer = 0.10 M Tris/Tris-HCl and 0.093−0.11 M NaCl (pH 8.0, ionic strength = 0.15 M at reaction temperature); $T = 27-37$ °C; $t = 1$ h; $V = 250$ μL. Data points (30−37 °C) are the average of 2 runs done in triplicate; data points (27 °C) are the average of 59 runs (control) and 19 runs (heparin) done in triplicate. (A) van't Hoff plot for standard enthalpy change, $\Delta H°$, of enzyme−substrate binding. Control (▲): $\Delta H° = -56 \pm 6$ kJ mol^{-1}; heparin (◇): $\Delta H°$ (app) $= -38 \pm 5$ kJ mol^{-1}. Lines were generated by the linear regression of data ($R^2 \geq 0.96$); $\Delta H°$ was calculated by equating the slope to $-\Delta H°/R$, where R is 8.314 J mol^{-1} K^{-1} (gas constant). (B) Arrhenius plot for energy of activation, E_a, for acylation of the ES complex. Control (▲): $E_a = 70.6 \pm 1.4$ kJ mol^{-1}; heparin (◇): E_a (app) $= 77 \pm 2$ kJ mol^{-1}. Lines were generated by the linear regression of data ($R^2 = 0.999$); E_a was calculated by equating the slope to $-E_a/R$.

or larger chains. Although the largest oligosaccharide tested was 22 saccharides long, the inclusion of data from the heparin preparations, which contain average chains of ~48 and ~60 saccharides, showed that α continued to increase with chain length. On the basis of these results, the trend in the inhibitory capacity of heparin-derived oligosaccharides and heparin preparations in terms of the number of saccharides is heparin (~60), heparin (~48) > 22 > 18, ~14 > 14 > ~12, 10, 8, and 4.

From the group of heparin-derived oligosaccharides, the 14 and 22 saccharides were selected for additional evaluation in concentration−response experiments. The results (Figure 5) supported tight-binding, hyperbolic inhibition similar to full-length heparin preparations. The smaller chains, however, were unable to attain the same level of maximum inhibition as heparin. The 14-saccharide-long chains reached a maximum inhibition of only 12% ($v_\infty/v_o = 0.88$). The slightly longer 22-saccharide chains reached a more substantial level of 29% ($v_\infty/v_o = 0.71$), but this was still less than the 56% maximum inhibition achieved by heparin. The K_i values were estimated by fitting the data to eq 1 assuming that 1 molecule of HNE binds to 1 molecule of heparin ($n = 1$). The values for the other parameters used in the nonlinear regression routine are summarized in Table 6. The results gave a best-fit value of K_i equal to 26 ± 10 nM for the 14 saccharide and 26 ± 9 nM for the 22 saccharide. This best-fit K_i is in the range of other K_i values reported in the literature for smaller chain heparins, for example, 20.7 ± 5.0 nM ($n = 1$) for a 5.0-kDa heparin fragment (16−18 saccharides) (*51*) and 40 nM for a heparin-derived oligosaccharide (16 saccharides) (*18*). A check of the $[E]_o/K_i$ ratio confirmed that both oligosaccharides were operating as tight-binding inhibitors (*32*). However, in comparison with the value of K_i determined for heparin (6.8 nM), the K_i for the 14 and 22 saccharides is 3.8-fold greater. This larger value of K_i implies that the shorter oligosaccharides are less effective in binding HNE than full-length heparin.

Table 4: Estimated Thermodynamic Properties from K_m and V_{max} for HNE Hydrolysis of Suc-Ala$_3$-*p*NA[a]

	enzyme−substrate binding step			acylation step
	$\Delta G°$ (kJ mol^{-1})[b]	$\Delta H°$ (kJ mol^{-1})[c]	$\Delta S°$ (kJ mol^{-1} K^{-1})[d]	E_a (kJ mol^{-1})[e]
control[f]	−16.05 ± 0.05	−56 ± 6	−0.13 ± 0.02	70.6 ± 1.4
heparin[g]	−12.79 ± 0.05	−38 ± 5	−0.085 ± 0.017	77 ± 2

[a] Reaction conditions: $[E]_o = 120$ nM; $[I]_o = 280$ nM (5.0 μg/mL; 17−19 kDa); $[S]_o = 0.30-7.2$ mM; buffer = 0.10 M Tris/Tris-HCl and 0.093−0.11 M NaCl (pH 8.0, ionic strength = 0.15 M at reaction temperature); $T = 27-37$ °C; $t = 1$ h; $V = 250$ μL. [b] Calculated from $\Delta G° = -RT \ln 1/K_m$ for 27 °C, with values of K_m from Table 1 and R equal to 8.314 J mol^{-1} K^{-1} (gas constant); estimated mean ± standard error of the mean. [c] Calculated from the slope ($-\Delta H°/R$) of the van't Hoff plot (Figure 3A) for 27−37 °C; best-fit value ± standard error. [d] Calculated from $\Delta G° = \Delta H° - T\Delta S°$ for 27 °C; uncertainty from propagation-of-error estimate. [e] Calculated from the slope ($-E_a/R$) of the Arrhenius plot (Figure 3B) for 27−37 °C; best-fit value ± standard error. Linear regression of data from both systems: $E_a = 74 \pm 2$ kJ mol^{-1}. [f] The control has no heparin. [g] Values for the heparin system are apparent thermodynamic properties.

Effect of Chemically Modified Heparins on HNE Hydrolysis. In Figure 6, the substrate−response results are shown for HNE hydrolysis of Suc-Ala$_3$-*p*NA in the presence of four chemically modified heparins. The ability of 2-O-, 6-O-, O-, and N-desulfated heparins to inhibit the reaction was evaluated at a concentration of 5.0 μg/mL for each compound (450 nM for O-desulfated heparin; 380 nM for the other heparins). The data from 2 to 5 runs for each modified heparin were processed in the same way as described for heparin (Figure 1) and are presented in the form of a double-reciprocal plot. The average best-fit values of K_m^{app} and V_{max}^{app} are listed in Table 7, together with the average values of the ratios K_m^{app}/K_m and V_{max}^{app}/V_{max}. For reference purposes, the plots of heparin and the control from Figure 1 are reproduced as dashed lines in Figure 6. From the common *y* intercept of all of the lines in Figure 6, it is apparent that the chemically modified heparins inhibit HNE by a competitive

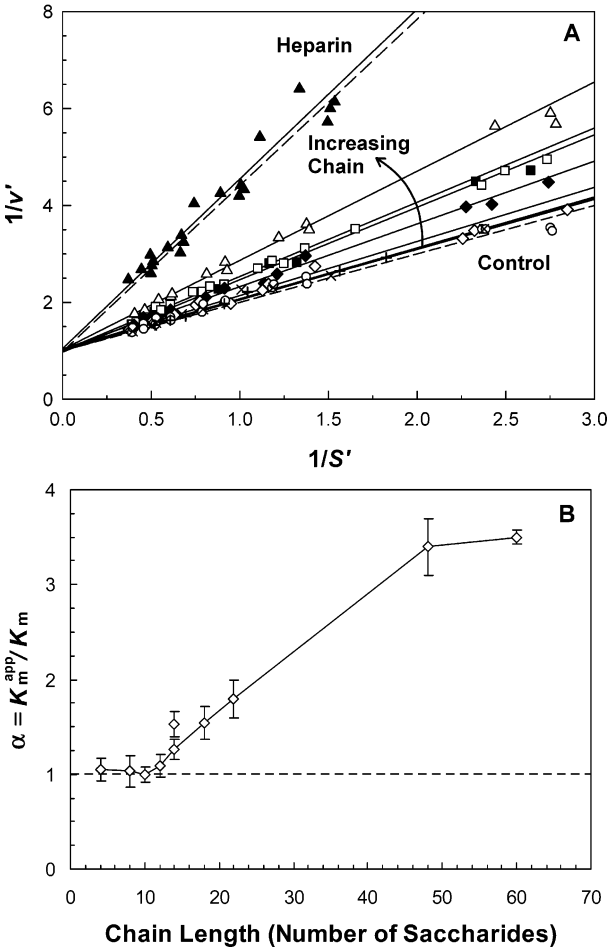

FIGURE 4: Inhibition of HNE hydrolysis by heparin-derived oligosaccharides. Reaction conditions: $[E]_o = 120$ nM; $[I]_o = 5.0$ μg/mL; $[S]_o = 0.60-3.6$ mM Suc-Ala$_3$-*p*NA; buffer = 0.10 M Tris/Tris-HCl and 0.093 M NaCl (pH 8.0, ionic strength = 0.15 M at 27 °C); $T = 27$ °C; $t = 1$ h; $V = 250$ μL. (A) Double-reciprocal plot. Data points (average of triplicate readings) are shown for 2−5 runs of each derivative: 4 saccharide, 4.2 μM (+); 8 saccharide, 2.1 μM (×); 10 saccharide, 1.7 μM (○); ∼12 saccharide, 1.4 μM (◇); 14 saccharide, 1.1 μM (◆); ∼14 saccharide, 1.2 μM (□); 18 saccharide, 0.83 μM (■); 22 saccharide, 0.68 μM (△); heparin (14−15 kDa), ∼48 saccharides, 0.34 μM (▲). Lines were generated from $1/v' = [(K_m^{app}/K_m)/(V_{max}^{app}/V_{max})]\ 1/S' + [1/(V_{max}^{app}/V_{max})]$ with average kinetic parameters from Table 5. Dashed lines are from Figure 1 for the control (lower - - -) and for heparin (17−19 kDa; ∼60 saccharides) (upper - - -). Normalized plot variables: $v' = v/V_{max}$; $S' = [S]_o/K_m$. (B) Plot of kinetic parameter $\alpha = K_m^{app}/K_m$ versus the chain length (number of saccharides). Reaction conditions are the same as for Figure 4A. Error bars were determined from the propagation-of-error estimate.

mechanism. This is reinforced by the results in Table 7, which show that all K_m^{app}/K_m values are greater than 1 and that all V_{max}^{app}/V_{max} values are approximately equal to 1.

Examination of the slopes in Figure 6 indicates that the chemically modified heparins were not as effective as heparin in inhibiting HNE hydrolysis. Although the modified heparins (11−13 kDa) have a lower molecular mass than the 17−19 kDa heparin, the closeness of the results for this latter heparin and the 14−15 kDa heparin in Figure 4 suggests that the overriding factor responsible for the decreased inhibition is the change in sulfate content and not the lower molecular mass. The data clearly show that each class of sulfation within heparin contributes to the overall inhibitory response and that loss of any sulfate moiety has a detrimental effect on the inhibitory process. The least important sulfate for inhibition was the 2-*O*-sulfate on the iduronic acid residue. Although loss of the 2-*O*-sulfate groups produced some reduction in inhibitory activity compared with heparin, 2-O-desulfated heparin was a much more effective inhibitor than the other modified heparins. Removal of either the *N*-sulfate or the 6-*O*-sulfate from the glucosamine residue appeared to be more critical to inhibition. The values of K_m^{app}/K_m for 6-O-desulfated heparin and N-desulfated heparin were about 2-fold less than the value for heparin. While 6-O-desulfated heparin reduced inhibition slightly more than N-desulfated heparin, the true potency of 6-*O*-sulfate groups was not clear, considering that the process to make the derivative removes a small percentage of other *O*-sulfate groups. Fully O-desulfated heparin performed about the same as 6-O-desulfated heparin in disrupting inhibition. In summary, the general trend for effectiveness at inhibiting HNE is heparin > 2-O-desulfated > N-desulfated > 6-O-desulfated, O-desulfated.

To represent the range of inhibition observed for the chemically modified heparins, N-desulfated heparin and 2-O-desulfated heparin were chosen for further evaluation in a series of concentration−response experiments (Figure 7). The trend of the HNE reaction kinetics in the presence of either N-desulfated heparin or 2-O-desulfated heparin was characteristic of tight-binding, hyperbolic inhibition. However, in comparison with heparin, the modified heparins leveled off at lower values of inhibition. Maximum inhibition dropped from 56% for heparin to 45% ($v_\infty/v_o = 0.55$) for 2-O-desulfated heparin and to only 29% ($v_\infty/v_o = 0.71$) for N-desulfated heparin. The curves in Figure 7 were generated by nonlinear regression of the data to eq 1 with all of the parameters fixed except K_i. With n assumed equal to 3.2, the resulting best-fit values for K_i were 169 ±18 nM for N-desulfated heparin and 66 ± 9 nM for 2-O-desulfated heparin. A summary of the parameters used in fitting both sets of data is provided in Table 8. The effect on K_i of assuming a smaller n of 2 is also included in the table.

A comparison of the K_i values for heparin ($K_i = 6.8$ nM) and the two chemically modified heparins showed that K_i increased as sulfate moieties were removed, reflecting poorer binding of the modified heparin to the elastase surface. Nevertheless, a check of the $[E]_o/K_i$ ratios confirmed that both modified heparins were still functioning within the range of tight-binding inhibitors (*32*). On the basis of the assumption of a constant binding stoichiometry ($n = 3.2$), the N-desulfated heparin had a 25-fold greater K_i compared with heparin, whereas 2-O-desulfated heparin had a 10-fold greater K_i. Thus, the removal of *N*-sulfate groups had a 2.5-fold greater effect on K_i than the removal of 2-*O*-sulfate groups.

Effect of Heparin Derivatives on HNE Elastolysis. To determine the extent to which the results obtained with synthetic substrate would relate to a more physiologically relevant reaction, various heparin derivatives were evaluated for their ability to inhibit HNE solubilization of elastin. The concentrations of HNE (120 nM) and inhibitor (5.0 μg/mL) were set at the same values as used in the synthetic substrate assays. Figure 8A shows the results for selected heparin-derived oligosaccharides together with the two heparin preparations. Although oligosaccharides up to 10 saccharides in length were not active, a slightly longer chain of ∼12

Table 5: Kinetic Parameters for the Inhibition of HNE Hydrolysis by Heparin-Derived Oligosaccharides[a]

oligosaccharide[b]	runs[c]	K_m^{app} (mM)	V_{max}^{app} (10^{-8} M s^{-1})	k_{cat}^{app} [d] (s^{-1})	k_{cat}^{app}/K_m^{app} (M^{-1} s^{-1})	α K_m^{app}/K_m	β V_{max}^{app}/V_{max}
4	2	1.56 ± 0.17[e]	4.20 ± 0.18	0.350 ± 0.019	230 ± 20	1.05 ± 0.12	1.00 ± 0.06
8	2	1.6 ± 0.2	4.5 ± 0.2	0.38 ± 0.02	230 ± 30	1.03 ± 0.17	0.98 ± 0.08
10	4	1.54 ± 0.08	4.09 ± 0.09	0.341 ± 0.011	222 ± 14	1.00 ± 0.08	0.97 ± 0.04
~12	3	1.62 ± 0.14	4.20 ± 0.16	0.350 ± 0.016	220 ± 20	1.09 ± 0.12	0.98 ± 0.05
14	3	1.86 ± 0.11	4.28 ± 0.11	0.356 ± 0.014	191 ± 14	1.26 ± 0.11	0.97 ± 0.04
~14	4	2.48 ± 0.18	4.57 ± 0.17	0.381 ± 0.017	154 ± 13	1.53 ± 0.13	1.00 ± 0.04
18	2	2.29 ± 0.11	4.60 ± 0.12	0.384 ± 0.016	168 ± 11	1.54 ± 0.17	1.03 ± 0.05
22	2	2.80 ± 0.12	4.53 ± 0.11	0.377 ± 0.016	135 ± 8	1.79 ± 0.19	0.98 ± 0.06
~48[f]	5	5.5 ± 0.4	4.27 ± 0.19	0.356 ± 0.017	64 ± 5	3.4 ± 0.3	0.96 ± 0.05

[a] Reaction conditions: $[E]_o$ = 120 nM; $[I]_o$ = 5.0 μg/mL (4.2 μM for 4 saccharide; 2.1 μM for 8 saccharide; 1.7 μM for 10 saccharide; 1.4 μM for ~12 saccharide; 1.1 μM for 14 saccharide; 1.2 μM for ~14 saccharide; 0.83 μM for 18 saccharide; 0.68 μM for 22 saccharide; 0.34 μM for heparin [14−15 kDa; ~48 saccharides]); $[S]_o$ = 0.60−3.6 mM Suc-Ala$_3$-*p*NA; buffer = 0.10 M Tris/Tris-HCl and 0.093 M NaCl (pH 8.0, ionic strength = 0.15 M at 27 °C); T = 27 °C; t = 1 h; V = 250 μL. [b] Number of saccharide units. [c] Number of runs; each run done in triplicate. [d] $k_{cat}^{app} = V_{max}^{app}/[E]_o$. [e] Estimated mean ± uncertainty from propagation of error. [f] Heparin (14−15 kDa).

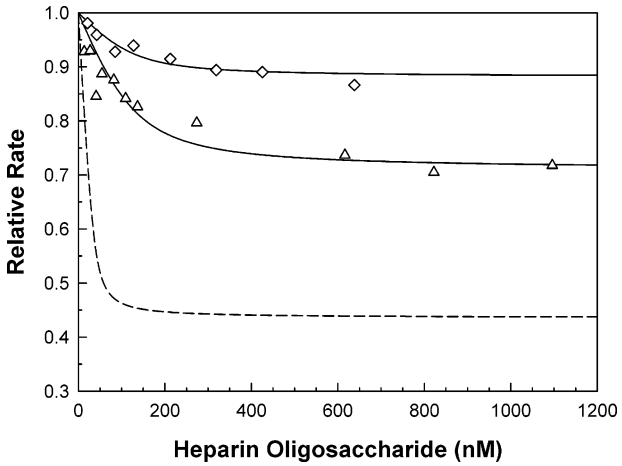

FIGURE 5: Concentration−response plot for the inhibition of HNE hydrolysis by heparin-derived oligosaccharides. Reaction conditions: $[E]_o$ = 120 nM; $[I]_o$ = 21−640 nM (0.10−3.0 μg/mL; 4.7 kDa) for 14 saccharide; $[I]_o$ = 14−2000 nM (0.10−14.5 μg/mL; 7.3 kDa) for 22 saccharide; $[S]_o$ = 1.5 mM Suc-Ala$_3$-*p*NA; buffer = 0.10 M Tris/Tris-HCl and 0.093 M NaCl (pH 8.0, ionic strength = 0.15 M at 27 °C); T = 27 °C; t = 1 h; V = 250 μL. Data points (average of triplicate readings) are shown for 2−3 runs of each derivative: 14 saccharide (◇); 22 saccharide (△). Solid curves were generated by fitting data to eq 1 by nonlinear regression with one adjustable parameter (K_i) and fixed parameters listed in Table 6. Best-fit values (n = 1): K_i = 26 ± 10 nM for 14 saccharide; K_i = 26 ± 9 nM for 22 saccharide. The dashed curve is from Figure 2A for heparin (17−19 kDa; ~60 saccharides). Relative rate (v_i/v_o) = (rate with heparin derivative)/(rate without heparin derivative); percent inhibition = $(1 - v_i/v_o) \times 100$.

saccharides (oligo I) inhibited at 16% (v_i/v_o = 0.84). Inhibition increased to 51% (v_i/v_o = 0.49) for a chain length of ~14 saccharides (oligo II) and reached a maximum of 92−95% (v_i/v_o = 0.05−0.08) for the larger heparin preparations (~48 and ~60 saccharides). From a comparison of Figure 8A with Figure 4, the general trend in the ability of the heparin oligosaccharides to inhibit HNE is similar in both the elastin and the synthetic substrate systems.

The chemically modified heparins were also evaluated in the elastin solubilization assay. As shown in Figure 8B, modified heparins inhibited the reaction to varying degrees but none of the compounds was as effective as heparin. The removal of *N*-sulfate groups produced the largest reduction in activity, decreasing the inhibition from 95% (v_i/v_o = 0.05) for heparin to only 29% (v_i/v_o = 0.71) for N-desulfated

Table 6: Nonlinear Regression Results for the Inhibition of HNE Hydrolysis by Heparin-Derived Oligosaccharides[a]

		fixed parameters[b]		best-fit values	
oligosaccharide[c]	adjustable parameters[d]	α	n	α	K_i (nM)
14	K_i	1.26	1		26 ± 10[e]
	K_i, α		1	1.31 ± 0.05	60 ± 30
22	K_i	1.79	1		26 ± 9
	K_i, α		1	1.79 ± 0.07	26 ± 13

[a] Experimental conditions: $[E]_o$ = 120 nM; $[I]_o$ = 21−640 nM (0.10−3.0 μg/mL; 4.7 kDa) for 14 saccharide; $[I]_o$ = 14−2000 nM (0.10−14.5 μg/mL; 7.3 kDa) for 22 saccharide; $[S]_o$ = 1.5 mM Suc-Ala$_3$-*p*NA; buffer = 0.10 M Tris/Tris-HCl and 0.093 M NaCl (pH 8.0, ionic strength = 0.15 M at 27 °C); T = 27 °C; t = 1 h; V = 250 μL. [b] Additional fixed parameters: $[E]_o$ = 120 nM; K_m = 1.61 mM; β = 1; $[S]_o$ = 1.5 mM; M_r = 4700 for 14 saccharide; M_r = 7300 for 22 saccharide. [c] Number of saccharide units. [d] Best estimates of K_i were obtained from nonlinear regression with one adjustable parameter. Nonlinear regression with two adjustable parameters (K_i, α) was limited to checking experimental values of α. Best-fit values of α were within error of experimental values (Table 5). [e] Best-fit value ± standard error.

heparin. In contrast, the loss of 2-*O*-sulfate groups was not as significant, and inhibition by 2-O-desulfated heparin remained fairly high at 76% (v_i/v_o = 0.24). The results for 6-O-desulfated heparin and O-desulfated heparin fell between these two extremes at about 46% inhibition (v_i/v_o = 0.54). In general, the inhibition of elastolysis by chemically modified heparins is consistent with the relative ability of these compounds to inhibit HNE hydrolysis of the synthetic substrate (Figure 6).

The similarity in the structural criteria for heparin inhibition of HNE activity, despite the significant difference between the structure of elastin and the synthetic substrate, indicates that the action of heparin is primarily mediated by interactions with the enzyme and is not dependent upon interactions between heparin and the substrate.

Molecular-Docking Analysis of Heparin Interactions with HNE. Parts A and B of Figure 9 show two views of the HNE molecule. The "front" view (Figure 9A) is oriented so that the catalytic site (Ser 195, His 57, and Asp 102) is in the center of the molecule. As indicated by the dashed line, the catalytic triad lies across the elastase fold, a crevice created by the juxtaposition of two barrel-like domains. A total of 19 arginine (Arg) residues are on the surface of the HNE molecule, and many of these positively charged residues are in the vicinity of the fold. The upper and lower

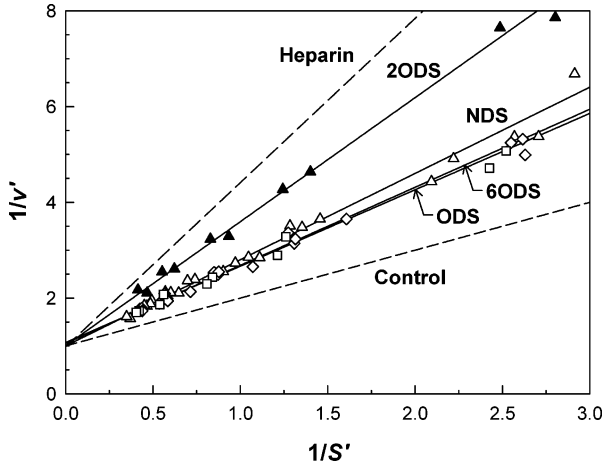

FIGURE 6: Double-reciprocal plot for the inhibition of HNE hydrolysis by chemically modified heparins. Reaction conditions: $[E]_o = 120$ nM; $[I]_o = 5.0$ μg/mL (450 nM for O-desulfated heparin, 11 kDa; 380 nM for other modified heparins, 13 kDa); $[S]_o = 0.6-3.6$ mM Suc-Ala$_3$-*p*NA; buffer = 0.10 M Tris/Tris-HCl and 0.093 M NaCl (pH 8.0, ionic strength = 0.15 M at 27 °C); $T = 27$ °C; $t = 1$ h; $V = 250$ μL. Data points (average of triplicate readings) are shown for 2−5 runs of each derivative: 2ODS, 2-O-desulfated heparin (▲); NDS, N-desulfated heparin (△); 6ODS, 6-O-desulfated heparin (◇); ODS, O-desulfated heparin (□). Lines were generated from $1/v' = [(K_m^{app}/K_m)/(V_{max}^{app}/V_{max})]\ 1/S' + [1/(V_{max}^{app}/V_{max})]$ with average kinetic parameters from Table 7. Dashed lines are from Figure 1 for the control (lower - - -) and for heparin (17−19 kDa) (upper - - -). Normalized plot variables: $v' = v/V_{max}$; $S' = [S]_o/K_m$.

ends of the fold appear to terminate in clusters of Arg residues. A better view of the Arg clusters can be obtained if the molecule is rotated 90° clockwise around the vertical axis, as shown by the "side" view (Figure 9B). From this vantage, each of the Arg clusters resolves into a clamp-like arrangement. The bottom clamp consists of Arg 36 and Arg 65 in the front and Arg 75, Arg 76, and Arg 80 in the back. The top clamp has Arg 177 and Arg 178 in the front and Arg 128 and Arg 129 in the back. The distance between the clamps is approximately 5 nm (50 Å), and the active site lies halfway between them.

In the top 10 docking results for heparin hexasaccharide ($^1C_4$ form) and HNE, the predictions showed the hexasaccharide in contact with arginine residues in various locations on the elastase surface. A majority of the complexes placed some portion of the hexasaccharide in either the bottom or top clamp. Two examples of the docking predictions are illustrated in parts C and D of Figure 9. For the complex in Figure 9C, the hexasaccharide has six ionic contacts between sulfate groups and Arg residues. The reducing end is in contact with Arg 147 and Arg 149, and the nonreducing end is in contact with Arg 36, Arg 75, Arg 76, and Arg 80 (bottom clamp). For the complex in Figure 9D, there are four ionic contacts with sulfate groups, two at the nonreducing end, Arg 129 and Arg 178 (top clamp), and two at the reducing end, Arg 177 (top clamp) and Arg 217. As apparent from these numerous ionic bonds, the clamp-like regions provide effective binding sites for the hexasaccharide. However, because the chain is short, about 2.5 nm (25 Å) in length, the hexasaccharide would be unable to extend into the active-site area and interfere with substrate binding.

Similar to the results for the smaller oligosaccharide, the top 10 docking complexes for heparin dodecasaccharide ($^1C_4$ form) and HNE showed the dodecasaccharide in close association with various arginine residues on the elastase surface. The longer chain increased the possibility that the docked oligosaccharide would interfere with the active site. For example, the predicted complex in Figure 9E shows the dodecasaccharide lying in the elastase fold. The linear structure of the dodecasaccharide is well-suited for the crevice-like area between domains, and the length of 5 nm (50 Å) is almost long enough to span the face of the HNE molecule. In addition to the physical fit, the dodecasaccharide is anchored at both ends by ionic contacts between sulfate groups and Arg residues, two at the reducing end with Arg 177 (top clamp) and two at the nonreducing end with Arg 36 (bottom clamp). A dodecasaccharide oriented in this manner on the HNE surface would be disruptive to any substrate molecule trying to bind in the active-site area.

Although the dodecasaccharide appears relatively secure in the docked position of Figure 9E, the molecule is too short to fully benefit from the increased stability of either of the two clamp-like regions at the ends of the elastase fold. Figure 9F shows an alternate structure from the docking results in which the dodecasaccharide is lodged lower in the fold, allowing the chain to pass through the bottom clamp in a way that might mimic a longer oligosaccharide. Despite the five saccharides (reducing end) that protrude freely from the bottom, the sugars remaining on the surface have a total of six ionic contacts between sulfate groups and Arg residues. Two of these contacts are at the nonreducing end with Arg 147 and Arg 149, and the remaining four contacts are with the bottom clamp (Arg 36, Arg 75, Arg 76, and Arg 80). Thus, because a heparin oligosaccharide is long enough to pass through the bottom clamp (or the top clamp), it becomes further stabilized in the elastase fold. An even longer oligosaccharide might possibly bind in both clamps. As a result of the increased stability, the oligosaccharide would reside on the surface for a longer time and have a greater opportunity to hinder substrate binding at the active site.

DISCUSSION

The initial promise that protease inhibitors would be effective for the treatment of emphysema has remained unfulfilled. As the true complexity of this disease has emerged, the need for a more comprehensive understanding of the molecular and cellular events is apparent. In the normal feedback mechanism of injury and repair in the lung, fragmented HSPGs from the destroyed extracellular matrix and damaged cells are believed to interact with elastases to limit their activity. An imbalance in the HSPG−elastase response potentially plays an important role in situations where uncontrolled lung injury leads to disease. Consequently, a more detailed understanding of the underlying mechanism of heparin and heparan sulfate inhibition of elastase will provide important insight into the complex process of lung injury and repair. Toward this end, the present investigation defines the kinetics and chemical requirements for heparin-mediated inhibition of HNE. The results demonstrate that heparin acts as a tight-binding, hyperbolic, competitive inhibitor of HNE and that this inhibition is strongly dependent upon polysaccharide chain length and degree of sulfation. These studies provide a critical step toward understanding how natural components of the lung (HSPGs) might contribute to regulating injury.

Table 7: Kinetic Parameters for the Inhibition of HNE Hydrolysis by Chemically Modified Heparins[a]

modified heparin	runs[b]	K_m^{app} (mM)	V_{max}^{app} (10^{-8} M s^{-1})	k_{cat}^{app} [c] (s^{-1})	k_{cat}^{app}/K_m^{app} (M^{-1} s^{-1})	α K_m^{app}/K_m	β V_{max}^{app}/V_{max}
2-O-desulfated	2	4.1 ± 0.3[d]	4.2 ± 0.2	0.35 ± 0.02	86 ± 8	2.6 ± 0.4	1.00 ± 0.07
6-O-desulfated	4	2.54 ± 0.13	4.06 ± 0.11	0.338 ± 0.012	133 ± 8	1.55 ± 0.16	0.95 ± 0.04
O-desulfated	2	2.22 ± 0.18	3.99 ± 0.16	0.333 ± 0.017	151 ± 13	1.49 ± 0.15	0.93 ± 0.04
N-desulfated	5	2.70 ± 0.19	4.32 ± 0.16	0.360 ± 0.015	134 ± 11	1.80 ± 0.14	1.00 ± 0.04

[a] Reaction conditions: $[E]_o = 120$ nM; $[I]_o = 5.0$ μg/mL (450 nM for O-desulfated heparin, 11 kDa; 380 nM for other modified heparins, 13 kDa); $[S]_o = 0.6-3.6$ mM Suc-Ala$_3$-*p*NA; buffer = 0.10 M Tris/Tris-HCl and 0.093 M NaCl (pH 8.0, ionic strength = 0.15 M at 27 °C); $T = 27$ °C; $t = 1$ h; $V = 250$ μL. [b] Number of runs; each run done in triplicate. [c] $k_{cat}^{app} = V_{max}^{app}/[E]_o$. [d] Estimated mean ± uncertainty from propagation of error.

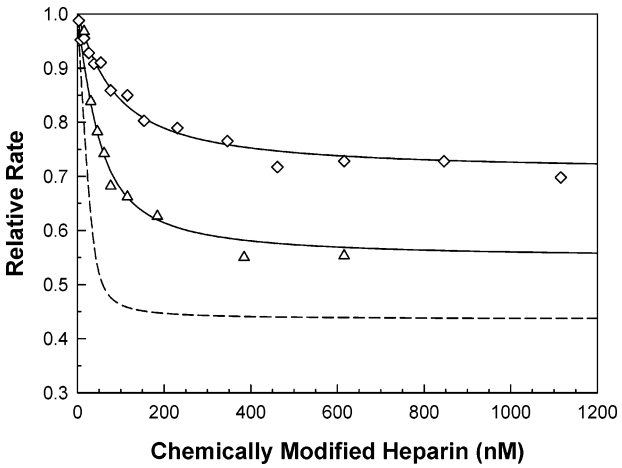

FIGURE 7: Concentration−response plot for the inhibition of HNE hydrolysis by chemically modified heparins. Reaction conditions: $[E]_o = 120$ nM; $[I]_o = 15-620$ nM (0.20−8.0 μg/mL; 13 kDa) for 2-O-desulfated heparin; $[I]_o = 3.1-1100$ nM (0.040−14.5 μg/mL; 13 kDa) for N-desulfated heparin; $[S]_o = 1.5$ mM Suc-Ala$_3$-*p*NA; buffer = 0.10 M Tris/Tris-HCl and 0.093 M NaCl (pH 8.0, ionic strength = 0.15 M at 27 °C); $T = 27$ °C; $t = 1$ h; $V = 250$ μL. Data points (average of triplicate readings) are shown for 2−3 runs of each derivative: 2-O-desulfated heparin (△); N-desulfated heparin (◇). Solid curves were generated by fitting data to eq 1 by nonlinear regression with one adjustable parameter (K_i) and fixed parameters listed in Table 8. Best-fit values ($n = 3.2$): $K_i = 66 \pm 9$ nM for 2-O-desulfated heparin; $K_i = 169 \pm 18$ nM for N-desulfated heparin. The dashed curve is from Figure 2A for heparin (17−19 kDa). Relative rate (v_i/v_o) = (rate with heparin derivative)/(rate without heparin derivative); percent inhibition = $(1 - v_i/v_o) \times 100$.

Mechanism of Heparin Inhibition of HNE Hydrolysis. The kinetic results of this study show that 1 molecule of heparin (17−19 kDa) binds to approximately 3 molecules of HNE ($n = 3.2$) with a K_i of 6.8 ± 1.8 nM (Figure 2 and Table 2). The inhibition is incomplete even at high concentrations of heparin, where the residual activity levels off at 0.44 (or 56% inhibition). The presence of heparin interferes with substrate binding at the active site, increasing K_m by a factor of 3.5. At the same time, the catalytic reaction rate is unaffected and V_{max} remains unchanged (Figure 1 and Table 1).

The competitive feature of this mechanism ($\alpha > 1$ and $\beta = 1$) is somewhat controversial in view of the noncompetitive mechanism cited by many published reports on heparin inhibition of HNE (*15*, *18*−*20*, *22*). However, the general acceptance of a noncompetitive mechanism is based on a limited amount of published data (*15*, *18*). When elastase assays were run under conditions modified to match various conditions in these reports, a competitive mechanism was found in each instance (Table 3). Competitive inhibition was also indicated for the heparin-derived oligosaccharides and chemically modified heparins of this study (Figures 4A and 6). Thus, the extensive set of kinetic data in the present report solidly supports the competitive aspect of heparin inhibition of HNE under the given experimental conditions.

Table 8: Nonlinear Regression Results for the Inhibition of HNE Hydrolysis by Chemically Modified Heparins[a]

modified heparin	adjustable parameters[c]	fixed parameters[b] α	fixed parameters[b] n	best-fit values α	best-fit values K_i (nM)
2-O-desulfated	K_i	2.6	3.2		66 ± 9[d]
	K_i	2.6	2		28 ± 4
	K_i, α		3.2	2.81 ± 0.17	82 ± 16
N-desulfated	K_i	1.80	3.2		169 ± 18
	K_i	1.80	2		91 ± 11
	K_i, α		3.2	1.88 ± 0.05	210 ± 30

[a] Experimental conditions: $[E]_o = 120$ nM; $[I]_o = 15-620$ nM (0.20−8.0 μg/mL; 13 kDa) for 2-O-desulfated heparin; $[I]_o = 3.1-1100$ nM (0.040−14.5 μg/mL; 13 kDa) for N-desulfated heparin; $[S]_o = 1.5$ mM Suc-Ala$_3$-*p*NA; buffer = 0.10 M Tris/Tris-HCl and 0.093 M NaCl (pH 8.0, ionic strength = 0.15 M at 27 °C); $T = 27$ °C; $t = 1$ h; $V = 250$ μL. [b] Additional fixed parameters: $[E]_o = 120$ nM; $K_m = 1.61$ mM; $\beta = 1$; $[S]_o = 1.5$ mM; $M_r = 13\,000$. [c] Best estimates of K_i ($n = 3.2$) were obtained from nonlinear regression with one adjustable parameter. Runs were repeated with $n = 2$ to examine the effect of fewer binding sites. Nonlinear regression with two adjustable parameters (K_i, α) was limited to checking experimental values of α. Best-fit α values were within error of experimental values (Table 7). [d] Best-fit value ± standard error.

Molecular-docking simulations provide a plausible physical model for the tight-binding, hyperbolic, competitive mechanism suggested by the kinetic analysis. According to the proposed bridging model, heparin is stabilized in the elastase fold by clamp-like clusters of arginine residues at the ends of the crevice (Figure 9). As these positively charged "clamps" tightly bind the negatively charged sulfate groups on heparin, the intervening chain extends across the active site. When the active site is bridged between the two clamps, heparin is able to sterically hinder substrate binding in a competitive manner. This situation is consistent with the greater maximal inhibition observed for the insoluble elastin substrate compared with the synthetic substrate. In the dynamic heparin−elastase equilibrium, the smaller synthetic substrate would be able to maneuver more easily around the heparin and take advantage of opportunities to slip into the active site.

Effect of Heparin Oligosaccharides on HNE Hydrolysis. Kinetic results with both synthetic and insoluble elastin substrates show that a minimum length of 12−14 saccharides is required for the inhibition of HNE (Figures 4 and 8A). Once this critical size is reached, the activity increases with the chain length (or molecular mass) of the heparin oligosac-

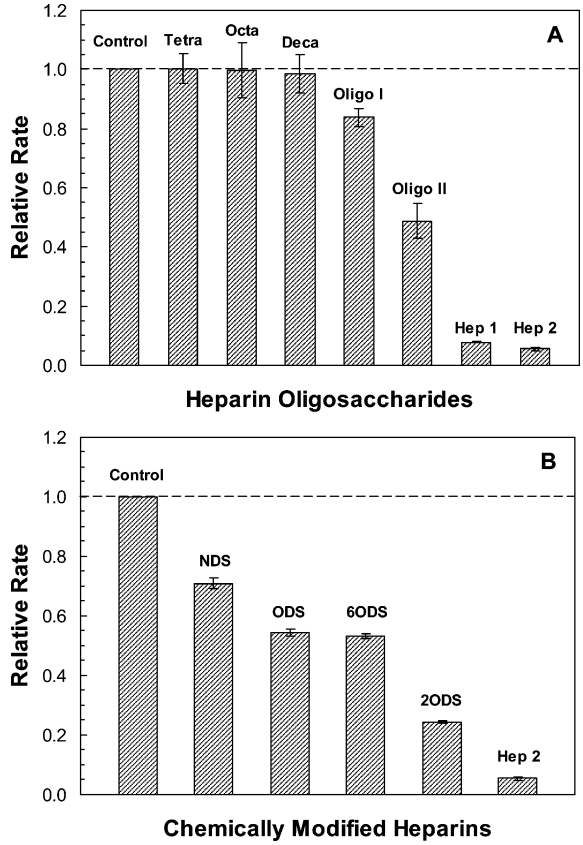

FIGURE 8: Inhibition of HNE elastolysis by heparin derivatives. Reaction conditions: $[E]_o$ = 120 nM; $[I]_o$ = 5.0 μg/mL; $[S]_o$ = 1.0 mg/mL ^{3}H-elastin; buffer = Dulbecco's PBS without calcium and magnesium salts (pH 7.1, ionic strength = 0.15 M); T = 37 °C; t = 2 h; V = 1 mL. The bar height was calculated from the average of triplicate readings; error bars were determined from the propagation-of-error estimate. Relative rate (v_i/v_o) = (^{3}H-elastin digestion with heparin derivative)/(^{3}H-elastin digestion without heparin derivative); percent inhibition = $(1 - v_i/v_o) \times 100$. (A) Relative rates for heparin-derived oligosaccharides. Control = no heparin derivative; Tetra = 4 saccharide (4.2 μM); Octa = 8 saccharide (2.1 μM); Deca = 10 saccharide (1.7 μM); Oligo I = ~12 saccharide (1.4 μM); Oligo II = ~14 saccharide (1.2 μM); Hep 1 = heparin (14−15 kDa; ~48 saccharides; 0.34 μM); Hep 2 = heparin (17−19 kDa; ~60 saccharides; 0.28 μM). (B) Relative rates for chemically modified heparins. Control = no heparin derivative; NDS = N-desulfated heparin (0.38 μM); ODS = O-desulfated heparin (0.45 μM); 6ODS = 6-O-desulfated heparin (0.38 μM); 2ODS = 2-O-desulfated heparin (0.38 μM); Hep 2 = heparin (17−19 kDa; 0.28 μM).

charide or heparin preparation. For the Suc-Ala$_3$-*p*NA substrate, inhibition follows a tight-binding, hyperbolic, competitive mechanism with enhanced values of K_m and unchanged values of V_{max} (Figure 4A and Table 5). The increase in K_m (or α) is directly proportional to the chain length for the 12−22 saccharides and continues to increase with chain length up to the higher molecular mass of the heparin preparations (Figure 4B). If binding with elastase is assumed to be 1:1 (n = 1), the oligosaccharides in the 14−22-saccharide range have a K_i of 26 ± 10 nM, which is 3.8-fold greater than the value determined for the heparin preparation (17−19 kDa) of ~60 saccharides (Figure 5 and Table 6).

The proposed bridging model can be used to interpret the kinetic results for the heparin-derived oligosaccharides. From the predicted docking complexes, a dodecasaccharide appears to be the minimum length that can both span the active site

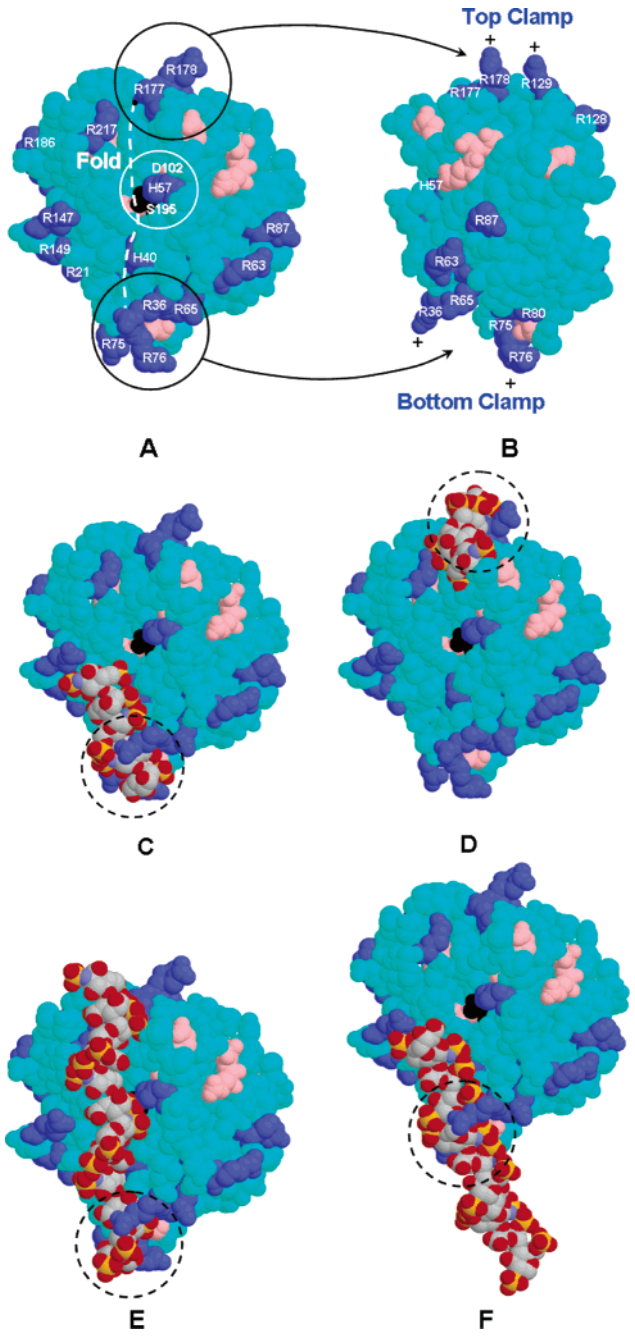

FIGURE 9: Molecular-docking results for heparin and HNE. Structure files were obtained from the PDB for heparin dodecasaccharide (1HPN) and HNE (1HNE). Docking complexes were generated by ZDOCK 2.3 and visualized with Protein Explorer 2.45. Atoms are shown as spheres of van der Waals radii. Color scheme for HNE residues: blue (basic), pink (acidic), black (Ser 195), and cyan (remainder). Color scheme for heparin atoms: gray (carbon), red (oxygen), blue (nitrogen), and yellow (sulfur). (A) Front view of the HNE molecule showing the catalytic site in the center. Circled region (white line) identifies the catalytic triad (Ser 195, His 57, and Asp 102); dashed line represents the elastase fold; circled regions (black line) indicate arginine clusters at the ends of the fold. (B) Side view of the HNE molecule showing top and bottom clamp-like regions of arginine clusters. The view was obtained by rotating the molecule in Figure 9A by 90° clockwise around the vertical axis. (C) Predicted complex showing heparin hexasaccharide in the HNE bottom clamp (circled region). (D) Predicted complex showing heparin hexasaccharide in the HNE top clamp (circled region). (E) Predicted complex showing heparin dodecasaccharide in the elastase fold. Circled region indicates the area of the bottom clamp. (F) Predicted complex showing heparin dodecasaccharide in the HNE bottom clamp (circled region).

and be anchored at each end by ionic contacts (Figure 9E). Moreover, the model predicts that, as the chain length increases, the oligosaccharide will be further stabilized through increased binding interactions in one or more of the clamps (Figure 9F). As the oligosaccharide experiences increased stability and a longer residence time on the elastase surface, the substrate molecule would face greater steric hindrance in reaching the active site. This scheme correlates well with the kinetic results that show an onset of inhibition at 12−14 saccharides and an increase in inhibition with an initial increase in the chain length.

The continuing increase in inhibitory activity with chain length is difficult to explain with only the bridging model. As the chain becomes longer and extends freely into space, there are no additional contacts with the elastase surface to stabilize the oligosaccharide. However, because binding is nonspecific, the free chain provides a source of more binding sites in close proximity to the bound elastase. As the elastase dissociates under equilibrium dynamics, it can immediately rebind in the microenvironment of the chain instead of diffusing into the reaction mixture to find another oligosaccharide. In this way, the elastase molecule can translate along the chain, dissociating and rebinding in an efficient manner that could hinder substrate binding. Thus, by the proposed bridging-translation model, as the chain becomes longer, increased binding and stability across the active site is coupled with an increased translation along the chain. While the first plays a role in the onset of inhibition and the initial increase in inhibition with chain length, the second could play a major role in the increase in inhibition with chain length.

Effect of Chemically Modified Heparins on HNE Hydrolysis. In kinetic studies using both synthetic and insoluble elastin substrates, the chemically modified heparins are less effective than heparin as inhibitors of HNE (Figures 6 and 8B). Because these preparations have fewer sulfate groups than the original heparin, their diminished potential as inhibitors was expected on the basis of reports in the literature (*15*, *18*, *19*). The level of activity of each modified heparin is dependent upon the specific sulfate groups present. Although each sulfate group contributes in a varying degree to the overall activity, the individual contributions are not necessarily additive (for example, 6-O-desulfated heparin versus O-desulfated heparin). The 2-*O*-sulfate groups are clearly less significant than either the *N*- or 6-*O*-sulfate groups. The relative ranking of the latter two groups varies, and while the 6-*O*-sulfate groups appear slightly more important with the synthetic substrate, the *N*-sulfate groups are certainly more important with the elastin substrate.

Regardless of the sulfation pattern, the chemically modified heparins inhibit HNE hydrolysis of Suc-Ala$_3$-*p*NA by a tight-binding, hyperbolic, competitive mechanism (Figures 6 and 7). Although molecular docking was not done with the modified heparins, the bridging model is still applicable for explaining the general trend in inhibition activity. As sulfate groups are removed from the heparin molecule, the anchoring of the chain across the active site becomes less secure. This is reflected in the increasing values of the experimentally determined K_i. If binding stoichiometry is assumed to be the same as with heparin ($n = 3.2$), K_i increases by 10-fold for 2-O-desulfated heparin (66 ± 9 nM) and 25-fold for N-desulfated heparin (169 ± 18 nM) under the conditions of this study (Table 8). Because the modified heparin is not as tightly bound to the elastase surface as heparin, the substrate molecule has a better chance of reaching the active site. The resulting values of K_m for the chemically modified heparins increase by factors of 1.5−2.6 (Table 7). Although these values are not as large as the apparent K_m for heparin, they definitely show varying amounts of steric hindrance at the binding site.

The structure of the heparin molecule may provide some clues for the relative influence of the three sulfate groups on inhibition. In the $^1C_4$ conformer of the heparin dodecasaccharide (*38*), the three sulfate groups are clustered in a linear arrangement on alternating sides of the molecule. The 2-*O*-sulfate group may have less influence on binding (and subsequently inhibition) because it is located between the other two sulfates. Although the loss of the 2-*O*-sulfate group would decrease the charge density of the cluster, it would not change the general interaction length of the cluster (∼0.85 nm), which is bracketed by the two end sulfates. In contrast, the loss of either the *N*- or 6-*O*-sulfate group would change both the charge density and the interaction length of the cluster. This combination of changes may result in a larger impact on binding that translates into a greater importance of *N*- and 6-*O*-sulfate groups to inhibition. Similar relationships are not as obvious in the $^2S_0$ conformer because the three sulfate groups are arranged in a triangular-shaped cluster.

The removal of the *N*-sulfate group also introduces other complications. Because the resulting N-unsubstituted group is an amino group (NH_3^+), the presence of a positive charge makes the modified heparin less negative than the other heparins having either the 2-*O*- or 6-*O*-sulfate group removed. The presence of the amino group may also modify the flexibility of the iduronate ring by restricting it to a deformed $^1C_4$ conformation (*52*). Both of these conditions, the positive charge and the reduction in the conformational freedom of the ring, would result in poorer binding with the elastase surface, providing an explanation for the significant loss of inhibitory activity with the N-desulfated heparin.

Effect of Heparin Derivatives on HNE Elastolysis. An interesting result of this study is the general similarity in trends between the synthetic substrate and the insoluble elastin substrate (Figures 4, 6, and 8). Other than the reduced activity of N-desulfated heparin with elastin, the relative effects of the heparin-derived oligosaccharides and the chemically modified heparins on inhibition of HNE hydrolysis are the same irrespective of the substrate. This is remarkable considering that one substrate is a small, soluble, tripeptide molecule and the other is an insoluble macromolecule. These results suggest that the major inhibitory action of heparin and heparin derivatives is through interactions with the elastase and not through interactions with the substrates.

In conclusion, the results of this comprehensive analysis provide new insights into the mechanism and structural requirements for the inhibition of HNE by heparin and heparin derivatives. The knowledge of these relationships will provide a strong basis for understanding the interactions that occur between elastase and elastase-generated HSPG fragments in the extracellular matrix of the lung. A breakdown of this natural feedback mechanism might result during conditions of chronic injury if HSPGs are depleted or incompletely modified during biosynthesis, which could

contribute to the progression of disease. The ability of heparin and HSPGs to modulate proteolytic activity indicates that this ubiquitous class of complex polysaccharides plays a central role in regulating tissue injury. Future studies will be required to more fully evaluate the role of endogenous HSPGs in regulating elastase-mediated tissue injury.

ACKNOWLEDGMENT

We are grateful to Dr. Antonio Baici (University of Zurich) for providing the elastase active-site titration method. We also thank Tina Seekri for her laboratory help and Gerald Coffman for his computer assistance.

REFERENCES

1. Pauwels, R. A., Buist, A. S., Calverley, P. M., Jenkins, C. R., and Hurd, S. S. (2001) Global strategy for the diagnosis, management, and prevention of chronic obstructive pulmonary disease. NHLBI/WHO Global Initiative for Chronic Obstructive Lung Disease (GOLD) Workshop summary, *Am. J. Respir. Crit. Care Med. 163*, 1256−1276.
2. Hedrick, H. L., and Kutscher, A. H. (2002) *The Quiet Killer. Emphysema/Chronic Obstructive Pulmonary Disease*, The Scarecrow Press, Inc., Lanham, MD.
3. National Heart, Lung, and Blood Institute (2003) *Chronic Obstructive Pulmonary Disease (COPD)*, U.S. Department of Health and Human Services, National Institutes of Health, Bethesda, MD. http://www.nhlbi.nih.gov/health/dci/Diseases/Copd/Copd_WhatIs.html.
4. Weiss, S. J. (1989) Tissue destruction by neutrophils, *N. Engl. J. Med. 320*, 365−376.
5. Janoff, A. (1985) Elastase in tissue injury, *Annu. Rev. Med. 36*, 207−216.
6. Damiano, V. V., Tsang, A., Kucich, U., Abrams, W. R., Rosenbloom, J., Kimbel, P., Fallahnejad, M., and Weinbaum, G. (1986) Immunolocalization of elastase in human emphysematous lungs, *J. Clin. Invest. 78*, 482−493.
7. Bernfield, M., Gotte, M., Park, P. W., Reizes, O., Fitzgerald, M. L., Lincecum, J., and Zako, M. (1999) Functions of cell surface heparan sulfate proteoglycans, *Annu. Rev. Biochem. 68*, 729−777.
8. Janoff, A. (1985) Elastases and emphysema. Current assessment of the protease−antiprotease hypothesis, *Am. Rev. Respir. Dis. 132*, 417−433.
9. Kainulainen, V., Wang, H., Schick, C., and Bernfield, M. (1998) Syndecans, heparan sulfate proteoglycans, maintain the proteolytic balance of acute wound fluids, *J. Biol. Chem. 273*, 11563−11569.
10. Shapiro, S. D., and Ingenito, E. P. (2005) The pathogenesis of chronic obstructive pulmonary disease: Advances in the past 100 years, *Am. J. Respir. Cell Mol. Biol. 32*, 367−372.
11. Turino, G. M. (2002) The origins of a concept: The protease−antiprotease imbalance hypothesis, *Chest 122*, 1058−1060.
12. Rao, N. V., Kennedy, T. P., Rao, G., Ky, N., and Hoidal, J. R. (1990) Sulfated polysaccharides prevent human leukocyte elastase-induced acute lung injury and emphysema in hamsters, *Am. Rev. Respir. Dis. 142*, 407−412.
13. Lafuma, C., Frisdal, E., Harf, A., Robert, L., and Hornebeck, W. (1991) Prevention of leucocyte elastase-induced emphysema in mice by heparin fragments, *Eur. Respir. J. 4*, 1004−1009.
14. Lever, R., and Page, C. P. (2002) Novel drug development opportunities for heparin, *Nat. Rev. Drug Discovery 1*, 140−148.
15. Baici, A., Diczhazi, C., Neszmelyi, A., Moczar, E., and Hornebeck, W. (1993) Inhibition of the human leukocyte endopeptidases elastase and cathepsin G and of porcine pancreatic elastase by *N*-oleoyl derivatives of heparin, *Biochem. Pharmacol. 46*, 1545−1549.
16. Frommherz, K. J., Faller, B., and Bieth, J. G. (1991) Heparin strongly decreases the rate of inhibition of neutrophil elastase by α 1-proteinase inhibitor, *J. Biol. Chem. 266*, 15356−15362.
17. Fryer, A., Huang, Y. C., Rao, G., Jacoby, D., Mancilla, E., Whorton, R., Piantadosi, C. A., Kennedy, T., and Hoidal, J. (1997) Selective O-desulfation produces nonanticoagulant heparin that retains pharmacological activity in the lung, *J. Pharmacol. Exp. Ther. 282*, 208−219.
18. Redini, F., Tixier, J. M., Petitou, M., Choay, J., Robert, L., and Hornebeck, W. (1988) Inhibition of leucocyte elastase by heparin and its derivatives, *Biochem. J. 252*, 515−519.
19. Volpi, N. (1996) Inhibition of human leukocyte elastase activity by heparins: Influence of charge density, *Biochim. Biophys. Acta 1290*, 299−307.
20. Walsh, R. L., Dillon, T. J., Scicchitano, R., and McLennan, G. (1991) Heparin and heparan sulphate are inhibitors of human leucocyte elastase, *Clin. Sci. 81*, 341−346.
21. Tian, Y., Gebitekin, C., Martin, P., Satur, C. M., Mearns, A., and Walker, D. R. (1995) Influence of heparin thromboprophylaxis on plasma leucocyte elastase levels following lobectomy for lung carcinoma, *Blood Coagulation Fibrinolysis 6*, 527−530.
22. Hornebeck, W., Lafuma, C., Robert, L., Moczar, M., and Moczar, E. (1994) Heparin and its derivatives modulate serine proteinases (SERPS) serine proteinase inhibitors (SERPINS) balance. Physiopathological relevance, *Pathol. Res. Pract. 190*, 895−902.
23. Gallagher, J. T. (2001) Heparan sulfate: Growth control with a restricted sequence menu, *J. Clin. Invest. 108*, 357−361.
24. Buczek-Thomas, J. A., and Nugent, M. A. (1999) Elastase-mediated release of heparan sulfate proteoglycans from pulmonary fibroblast cultures. A mechanism for basic fibroblast growth factor (bFGF) release and attenuation of bfgf binding following elastase-induced injury, *J. Biol. Chem. 274*, 25167−25172.
25. van de Lest, C. H., Versteeg, E. M., Veerkamp, J. H., and van Kuppevelt, T. H. (1995) Digestion of proteoglycans in porcine pancreatic elastase-induced emphysema in rats, *Eur. Respir. J. 8*, 238−245.
26. Baugh, R. J., and Travis, J. (1976) Human leukocyte granule elastase: Rapid isolation and characterization, *Biochemistry 15*, 836−841.
27. Stone, P. J., Crombie, G., and Franzblau, C. (1977) The use of tritiated elastin for the determination of subnanogram amounts of elastase, *Anal. Biochem. 80*, 572−577.
28. Wei, Y., and Pei, D. (1997) Continuous spectrophotometric assay of peptide deformylase, *Anal. Biochem. 250*, 29−34.
29. Lestienne, P., and Bieth, J. G. (1980) Activation of human leukocyte elastase activity by excess substrate, hydrophobic solvents, and ionic strength, *J. Biol. Chem. 255*, 9289−9294.
30. Baici, A. (1990) Interaction of human leukocyte elastase with soluble and insoluble protein substrates. A practical kinetic approach, *Biochim. Biophys. Acta 1040*, 355−364.
31. Snider, G. L., Stone, P. J., Lucey, E. C., Breuer, R., Calore, J. D., Seshadri, T., Catanese, A., Maschler, R., and Schnebli, H. P. (1985) Eglin-c, a polypeptide derived from the medicinal leech, prevents human neutrophil elastase-induced emphysema and bronchial secretory cell metaplasia in the hamster, *Am. Rev. Respir. Dis. 132*, 1155−1161.
32. Bieth, J. G. (1995) Theoretical and practical aspects of proteinase inhibition kinetics, *Methods Enzymol. 248*, 59−84.
33. Berman, H. M., Westbrook, J., Feng, Z., Gilliland, G., Bhat, T. N., Weissig, H., Shindyalov, I. N., and Bourne, P. E. (2000) The Protein Data Bank, *Nucleic Acids Res. 28*, 235−242.
34. Navia, M. A., McKeever, B. M., Springer, J. P., Lin, T. Y., Williams, H. R., Fluder, E. M., Dorn, C. P., and Hoogsteen, K. (1989) Structure of human neutrophil elastase in complex with a peptide chloromethyl ketone inhibitor at 1.84-Å resolution, *Proc. Natl. Acad. Sci. U.S.A. 86*, 7−11.
35. Bode, W., Wei, A. Z., Huber, R., Meyer, E., Travis, J., and Neumann, S. (1986) X-ray crystal structure of the complex of human leukocyte elastase (PMN elastase) and the third domain of the turkey ovomucoid inhibitor, *EMBO J. 5*, 2453−2458.
36. Wei, A. Z., Mayr, I., and Bode, W. (1988) The refined 2.3 Å crystal structure of human leukocyte elastase in a complex with a valine chloromethyl ketone inhibitor, *FEBS Lett. 234*, 367−373.
37. Hartley, B. S. (1964) Amino-acid sequence of bovine chymotrypsinogen A, *Nature 201*, 1284−1287.
38. Mulloy, B., Forster, M. J., Jones, C., and Davies, D. B. (1993) NMR and molecular-modelling studies of the solution conformation of heparin, *Biochem. J. 293* (part 3), 849−858.
39. Chen, R., Li, L., and Weng, Z. (2003) ZDOCK: An initial-stage protein-docking algorithm, *Proteins 52*, 80−87.
40. Chen, R., Tong, W., Mintseris, J., Li, L., and Weng, Z. (2003) ZDOCK predictions for the CAPRI challenge, *Proteins 52*, 68−73.
41. Li, L., Chen, R., and Weng, Z. (2003) RDOCK: Refinement of rigid-body protein docking predictions, *Proteins 53*, 693−707.

42. Martz, E. (2002) Protein Explorer: Easy yet powerful macromolecular visualization, *Trends Biochem. Sci. 27*, 107−109.
43. Ledoux, D., Papy-Garcia, D., Escartin, Q., Sagot, M. A., Cao, Y., Barritault, D., Courtois, J., Hornebeck, W., and Caruelle, J. P. (2000) Human plasmin enzymatic activity is inhibited by chemically modified dextrans, *J. Biol. Chem. 275*, 29383−29390.
44. Segel, I. H. (1993) *Enzyme Kinetics. Behavior and Analysis of Rapid Equilibrium and Steady-State Enzyme Systems*, John Wiley and Sons, Inc., New York.
45. Szedlacsek, S. E., Ostafe, V., Serban, M., and Vlad, M. O. (1988) A re-evaluation of the kinetic equations for hyperbolic tight-binding inhibition, *Biochem. J. 254*, 311−312.
46. Dennis, J. E., Jr., and Schnabel, R. B. (1996) *Numerical Methods for Unconstrained Optimization and Nonlinear Equations*, Society for Industrial and Applied Mathematics, Philadelphia, PA.
47. Williams, J. W., and Morrison, J. F. (1979) The kinetics of reversible tight-binding inhibition, *Methods Enzymol. 63*, 437−467.
48. Cadene, M., Duranton, J., North, A., Si-Tahar, M., Chignard, M., and Bieth, J. G. (1997) Inhibition of neutrophil serine proteinases by suramin, *J. Biol. Chem. 272*, 9950−9955.
49. Cha, S. (1975) Tight-binding inhibitors-I. Kinetic behavior, *Biochem. Pharmacol. 24*, 2177−2185.
50. Gutfreund, H. (1972) *Enzymes: Physical Principles*, John Wiley and Sons, Inc., New York.
51. Ermolieff, J., Boudier, C., Laine, A., Meyer, B., and Bieth, J. G. (1994) Heparin protects cathepsin G against inhibition by protein proteinase inhibitors, *J. Biol. Chem. 269*, 29502−29508.
52. van Boeckel, C. A. A., van Aelst, S. F., Wagenaars, G. N., Mellema, J.-R., Paulsen, H., Peters, T., Pollex, A., and Sinnwell, V. (1987) Conformational analysis of synthetic heparin-like oligosaccharides containing α-L-idopyranosyluronic acid, *Recl. Trav. Chim. Pays-Bas 106*, 19−29.

BI060338R